ADVANCED ENERGY MATERIALS
www.advenergymat.de

# Overview on Theoretical Simulations of Lithium-Ion Batteries and Their Application to Battery Separators

*Daniel Miranda, Renato Gonçalves, Stefan Wuttke, Carlos M. Costa,* and Senentxu Lanceros-Méndez*

**For the proper design and evaluation of next-generation lithium-ion batteries, different physical-chemical scales have to be considered. Taking into account the electrochemical principles and methods that govern the different processes occurring in the battery, the present review describes the main theoretical electrochemical and thermal models that allow simulation of the performance of lithium-ion batteries, including different materials and components (electrodes and separators) and battery geometries. As the separator plays an essential role in the performance and safety of lithium-ion batteries, the recent theoretical simulation work for this battery component are shown, with particular emphasis on morphology, dendrite growth, ionic transport, and mechanical properties. Further theoretical simulations and modeling of this battery component are still required for improving performance, taking into consideration varying geometric parameters such as pore size, porosity, and tortuosity as well as the optimization of the lithium diffusion process and ionic conductivity value. Theoretical simulations of battery separators will play an essential role in the new generation of lithium-ion batteries, allowing the improvement of their performance while reducing experimental probes and time.**

## 1. Introduction

The two topics, energy and environment, will be the most relevant global challenges that society will face for the years to come. Thus, the main focus of research and development should be to address these critical challenges by combining the two topics in order to achieve a new generation of environmentally friendlier energy technologies, focusing on clean generation, conversion, and storage.[1]

Since the first renewable energy generation system, important developments have been achieved not only in sustainable energy generation but also in energy storage systems. In the latter, electrochemical devices such as lithium-ion batteries are widely used for a large variety of applications, such as small portable electronic devices and electric vehicles, mainly based on their high energy density.[2] Lithium-ion batteries are therefore one of the most relevant energy storage devices due to their advantages when compared to other battery systems as they are cheaper, lighter, show higher energy density, have no memory effect, less self-discharge, higher number of charge/discharge cycles, and improved safety.[3] Lithium-ion batteries are typically based on three main components (anode, cathode, and separator) and two mains' processes (charge and discharge of the battery). These processes are driven by electrochemical processes, lithium-ion, and electrons movement between electrodes allowing to storage/deliver energy.[4]

With the need for further improving lithium-ion batteries as an efficient way to match the ever-developing needs of portable

D. Miranda
2Ai- School of Technology
IPCA
Barcelos 4750–810, Portugal
D. Miranda
LASI – Associate Laboratory of Intelligent Systems
Guimarães, Portugal
R. Gonçalves
Center of Chemistry
University of Minho
Braga 4710-057, Portugal

The ORCID identification number(s) for the author(s) of this article can be found under https://doi.org/10.1002/aenm.202203874.



**DOI: 10.1002/aenm.202203874**

S. Wuttke, S. Lanceros-Méndez
BCMaterials
Basque Center for Materials
Applications and Nanostructures
UPV/EHU Science Park, Leioa 48940, Spain
S. Wuttke, S. Lanceros-Méndez
IKERBASQUE
Basque Foundation for Science
Bilbao 48009, Spain
C. M. Costa
Physics Centre of Minho and Porto Universities (CF-UM-UP)
University of Minho
Braga 4710-057, Portugal
E-mail: cmscosta@fisica.uminho.pt
C. M. Costa
Laboratory of Physics for Materials and Emergent Technologies
LapMET
University of Minho
Braga 4710-057, Portugal
C. M. Costa
IB-S Institute of Science and Innovation for Sustainability
Universidade do Minho
Braga 4710-057, Portugal

device technologies, simulation, and computational modeling are essential tools for supporting the development and optimization of batteries and battery components.

Computational simulation of lithium-ion batteries has a significant impact on the prediction of the performance of these energy storage systems as well as on the behavior and bonding of elements generated during their use. This area of research promotes a deeper theoretical knowledge of the operation of the devices, and existing theoretical models supporting materials development by modeling the main processes that occur in the operation of the battery.[5] In this review, we wish to describe the recent framework and theoretical advances in modeling lithium-ion battery operation.

## 2. Theoretical Modeling and Simulations of Lithium-Ion Batteries

Theoretical models at the macro and micro-scales for lithium-ion batteries aim to describe battery operation through the electrochemical model at different battery dimensions and under several conditions. Studies have further implemented coupled models to evaluate thermal, mechanical, and magnetic parameters in correlation with the electrochemical variables. Thermal, mechanical, and magnetic models have been coupled to the electrochemical model, establishing proper interrelations between their corresponding parameters, as illustrated in **Figure 1**. In most coupled models, the Doyle/Fuller/Newman electrochemical model represents the base model that describes the electrochemical processes (Electrochemical Battery Model).

**Table 1** shows the main equations of the Doyle/Fuller/Newman electrochemical model that describe the electrochemical phenomena that occur in the battery components (current collectors, electrodes, and separator) during its operation processes. In the electrochemical model, liquid, solid, and porous phases are considered. The electrodes (cathode and anode) are studied as porous phase and the electrolyte is in a liquid phase and is present in the electrodes and separator pores.[6]

In the electrochemical model (Table 1), interpolation functions of several active materials parameters are introduced, such as the solid phase potential value ($\varphi_E$) as a function of the lithium-ion concentration in the electrode solid ($C_E$) and the potential value of the solid phase ($\varphi_E$) as a function of temperature (T). Regarding the electrolyte, interpolation functions of ionic conductivity ($K_l$) and lithium-ion concentration at the liquid phase ($C_L$) are also taken into account.

At all three cell components (anode, cathode, and separator) occurs the diffusion of lithium-ions through the electrolyte,

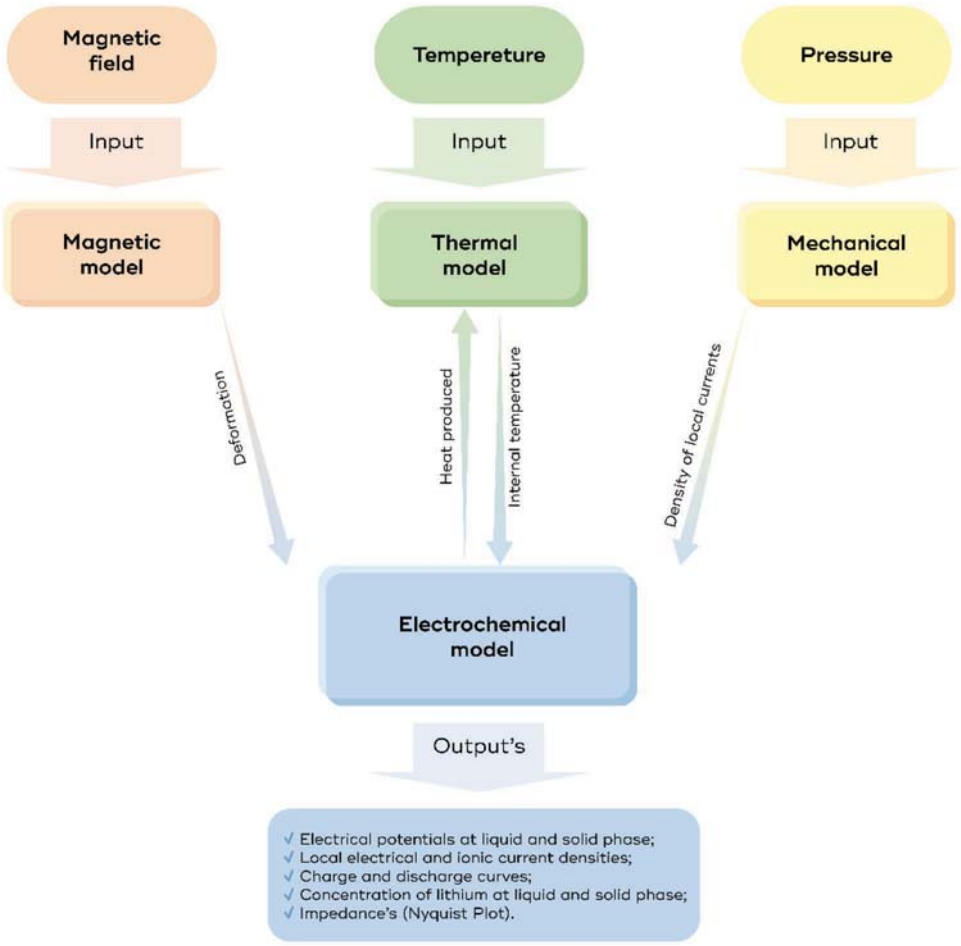


**Figure 1.** Different models coupled to the electrochemical model for the simulation of lithium-ion batteries.

**Table 1.** Main equations of Doyle/Fuller/Newman Electrochemical Model of the battery.[6] The identification of the symbols is provided in the nomenclature section.

| Battery Component | Equation | Description |
|---|---|---|
| Electrodes (Cathode and Anode) | $-\nabla.\,(\sigma_{ef,i}\nabla\varphi_E) = -FaJ_{Li+},\ i = a,c$ | Electrode potential calculated by the Ohm Law where the current density gradient is substituted by its equivalent in terms of lithium-ion flux according to Faraday's Laws. |
| | $-\nabla\,(K_{ef,i}\nabla\varphi_L) = FaJ_{Li^+} + \frac{2kRT}{F}(1-t_+^0)\nabla(\nabla\ln(C_L)), i = a,c$ | This equation relates the potential of the electrolyte with the local current density in the cathode and anode (Ohm Law). |
| | $\varepsilon_i\,\frac{\partial C_L}{\partial t} = \nabla(D_{ef,i}\nabla C_L) + a(1-t_+^0)J_{Li^+}, i = a,c$ | Diffusion of lithium ions in the electrolyte applied to the cathode and anode (Fick Diffusion Law). |
| | $\frac{\partial C_E}{\partial t} = D_{Li}\left[\frac{\partial^2 C_E}{\partial r^2} + \frac{2}{r}\frac{\partial C_E}{\partial r}\right]$ | Diffusion of lithium ions in the active material (solid phase) |
| | $D_{ef,i} = D_l\,\varepsilon_i^{brugg}$<br>$K_{ef,i} = K_l\,\varepsilon_i^{brugg}$<br>brugg = 1.5 and $i = a, c$<br>$\sigma_{ef,i} = \sigma_i\,(1-\varepsilon_i-\varepsilon_{f,i}),\ i = a, c$ | The effective ionic conductivity and diffusion in the liquid phase, applied to the cathode and anode, and the effective electrical conductivity in the solid phase. These parameters will depend on the porosity of the electrodes, $\varepsilon_i$, and the Bruggeman coefficient (brugg). |
| Separator | $-\nabla\,(K_{ef,s}\nabla\varphi_L) = FaJ_{Li^+} + \frac{2kRT}{F}(1-t_+^0)\nabla(\nabla\ln(C_L))$ | This equation relates the potential of the electrolyte with the local current density (Ohm Law). |
| | $\varepsilon_s\,\frac{\partial C_L}{\partial t} = \nabla.(D_{ef,s}\nabla C_L)$ | Lithium-ion diffusion in the electrolyte. |
| | $D_{ef,s} = D_l\,\varepsilon_s^{brugg}$<br>$K_{ef,s} = K_l\,\varepsilon_s^{brugg}$ | The effective diffusion and conductivity of the ions in the separator |
| **General Equations** | **Equation** | **Description** |
| Faraday's law (electrodes) | $\nabla\,i_E = -FaJ_{Li+}$ | Faraday's law express the relationship between the insertion/extraction of lithium ions into the electrodes with the electrical charge flow. Relation between the lithium ions flux and the current density in the electrodes. |
| Faraday's law (electrolyte) | $\nabla\,i_L = FaJ_{Li+}$ | Relation between the lithium ions flux and the current density in the electrolyte (Faraday' s Law). |
| Total current density (electrodes and electrolyte) | $i_E + i_L = I_{TOTAL}$ | Conservation of charge. The current density is preserved between the electrode and the electrolyte. |
| Butler–Volmer equation (kinetics) | $J_i = \left\{\exp\left(\frac{F(\eta-u^0)}{2RT}\right) - \exp\left(\frac{-F(\eta-u^0)}{2RT}\right)\right\}$<br>$i_{0,i} = k_i\,(C_{E,i}^{max} - C_{E,i}^S)^{\alpha_{a,i}}(C_{E,i}^S)^{\alpha_{c,i}}(C_L)^{\alpha_{a,i}}, i = a,c$ | Kinetics of the heterogeneous reaction at the electrode/electrolyte interface, described by the Butler–Volmer equation. |
| Variable over- potential | $\eta = \varphi_E - \varphi_L - u^0$ | The variable over-potential relates the potential of the electrodes/electrolyte and the open circuit voltage. |
| Overall mass balance. | $\frac{\partial C_L}{\partial t} = -\nabla.M + R$ | Overall mass balance. |
| Term of the reaction | $R = -\frac{a}{V_+}(1-t_+^0)J_{Li^+}$ | Reaction term of the mass balance equation. |
| Mass transport process | $M = -D(1-\frac{dlnC_{L_0}}{dlnC_L})\nabla C_L + \frac{i_L t_+^0}{F}$ | Mass transport flux. |

however, the current collectors are a wall impermeable to the electrolyte, so the flow of lithium-ions is null at these limits. The interfaces between the three components show a condition of continuity that is expressed as an equal mass that flows on both sides of the interface. **Table 2** shows the boundary conditions adopted for the different equations at the interfaces between the regions that will be presented for the battery model in 1D (**Figure 2**) where $L_a$, $L_s$, and $L_c$ are the width of the anode, separator, and cathode, respectively.

To evaluate the thermal parameters, thermal models are coupled,[8] allowing to measure the internal temperature reached by the battery and three important sources of heat produced by the

**Table 2.** Summary of the boundary conditions or limits of the mathematical model 1D adopted by.[7]

| | | Boundary Conditions | | | |
|---|---|---|---|---|---|
| Battery Component | Governing Law | $x = 0$ | $x = L_a$ | $x = L_a + L_s$ | $x = L_a + L_s + L_c$ |
| **Electrolyte** | $Li^+$ Diffusion | $\frac{\partial C_L}{\partial x} = 0$ | Continuity | Continuity | $\frac{\partial C_L}{\partial x} = 0$ |
| | Ohm's Law | $\varphi_L = \varphi_{L,0}$ | Continuity | Continuity | $\frac{\partial \varphi_L}{\partial x} = 0$ |
| **Electrodes** | Ohm's Law | $\varphi_E = 0$ | $\frac{\partial \varphi_E}{\partial x} = 0$ | $\varphi_E = \varphi_{E,0}$ | $\frac{\partial \varphi_E}{\partial x} = -\frac{I_{TOTAL}}{\sigma}$ |
| | **Governing Law** | **r = 0** | $r = R_S$ | | |
| | $Li^+$ Diffusion | $r = 0$ $\frac{\partial C_E}{\partial r} = 0$ | $r = R_S$ $\frac{\partial C_E}{\partial r} = -\frac{j_{Li+}}{D_{Li}}$ | | |

electrodes such as reversible and reaction heat and ohmic heat. Regarding the separator, the dissipated heat associated with internal resistance on charge transport can be measured. These models take into account heat exchanges with the external environment at several thermal conditions.

For the thermal model, several equations are applied describing the main thermal phenomena that occur at the different battery components (electrodes and electrolyte/separator). The following are the main equations governing the thermal behavior of the battery.[12–15] Equation (1) shows the energy balance in all battery components through the first law of thermodynamics:

$$\rho_I C_{p,i} \frac{dT}{dt} = \lambda_i \frac{\partial^2 T}{\partial x^2} + \lambda_i \frac{\partial^2 T}{\partial y^2} + Q_{total,i}, \; i = a,s,c \tag{1}$$

where $\rho$, $C_{p,I}$, and $\lambda_i$ are the density of battery components, heat capacity at constant pressure of battery components, and thermal conductivity of battery components, respectively. The $Q_{total,i}$ is the total heat generation rate at each battery component. For electrodes, the $Q_{total,i}$ is the sum of all heat produced by electrodes such as the total reaction heat generation (irreversible), $Q_{reaction,i}$, total reversible heat generation (reversible), $Q_{reversible,i}$, and total ohmic heat generation, $Q_{ohmic,i}$, and is expressed by Equation (2):

$$Q_{total,i} = Q_{reaction,i} + Q_{reversible,i} + Q_{ohmic,i}, \; i = a,c \tag{2}$$

The total reversible heat generation (reversible), $Q_{reversible,i}$, is related to the reversible entropy loss in electrodes, and the total reaction heat generation (irreversible), $Q_{reaction,i}$, is related to concentration polarization, activation polarization, and ohmic polarization. Equations (3) and (4) allow to determine, respectively, the reversible and irreversible heat generation produced by the electrodes.

$$Q_{reversible,i} = FaJT\frac{\partial U}{\partial T}, \; i = a,c \tag{3}$$

$$Q_{reaction,i} = FaJ(\varphi_E - \varphi_L - U), \; i = a,c \tag{4}$$

with the parameters $T$, $U$, $\varphi_E$, $\varphi_L$, $F$, $U$, and $dU/dT$, which represent the temperature, the open-circuit voltage, the potential of the electrodes, the potential of the electrolyte, the Faraday's constant, the open-circuit voltage and the coefficient of open-circuit voltage varying with temperature, respectively.

At the electrodes, the total ohmic heat generation, $Q_{ohmic,i}$, corresponds to the heat dissipated, produced by the internal resistance associated with the charge transport and is defined by the following Equation (5):

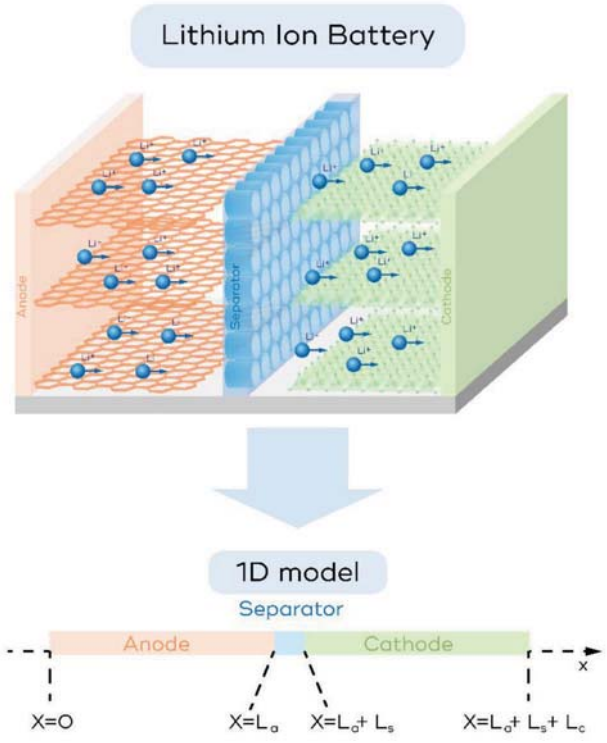


**Figure 2.** Schematic representation of the 1D model applied to lithium-ion batteries.

$$Q_{\text{ohmic},i} = \sigma_{\text{ef},i}\left(\frac{\partial\varphi_{\text{E}}}{\partial x}\right)^2 + \sigma_{\text{ef},i}\left(\frac{\partial\varphi_{\text{E}}}{\partial y}\right)^2 + k_{\text{ef},i}\left(\frac{\partial\varphi_{\text{L}}}{\partial x}\right)^2 + k_{\text{ef},i}\left(\frac{\partial\varphi_{\text{L}}}{\partial y}\right)^2 + \frac{2k_{\text{ef},i}RT}{F}(1-t_+)\frac{\partial(\ln c_i)}{\partial x}\frac{\partial\varphi_{\text{L}}}{\partial x} + \frac{2k_{\text{ef},i}RT}{F}(1-t_+)\frac{\partial(\ln c_i)}{\partial y}\frac{\partial\varphi_{\text{L}}}{\partial y},\ i=a,c \tag{5}$$

where $\sigma_{\text{ef},i}$ is the effective electronic conductivity of the solid phase of the electrode and $\kappa_{\text{ef},i}$ is the effective ionic conductivity of the electrolyte.

Regarding separator, the total heat generation, $Q_{\text{total},i}$, corresponds only to the contribution related to the total ohmic heat generation, $Q_{\text{ohmic},i}$, produced by the internal resistance associated with the flow of lithium-ions, as shown in Equation (6):

$$Q_{\text{total},i} = Q_{\text{ohmic},i},\ i=s \tag{6}$$

where the total ohmic heat generation, $Q_{\text{ohmic},i}$, produced at the separator is defined by the following Equation (7):

$$Q_{\text{ohmic},i} = k_{\text{ef},i}\left(\frac{\partial\varphi_{\text{L}}}{\partial x}\right)^2 + k_{\text{ef},i}\left(\frac{\partial\varphi_{\text{L}}}{\partial y}\right)^2 + \frac{2k_{\text{ef},i}RT}{F}(1-t_+)\frac{\partial(\ln c_i)}{\partial x}\frac{\partial\varphi_{\text{L}}}{\partial x} + \frac{2k_{\text{ef},i}RT}{F}(1-t_+)\frac{\partial(\ln c_i)}{\partial y}\frac{\partial\varphi_{\text{L}}}{\partial y},\ i=s \tag{7}$$

The electrochemical parameters of electrodes such as open circuit potential, $U$, reaction rate coefficient, $k_{\text{Li}}$, and diffusion coefficient of Li ions, $D_{\text{Li}}$, as a function of temperature are shown in Equations (8)–(10), respectively,

$$U_i = U_{\text{ref},i} + (T - T_{\text{ref}})\left[\frac{\text{d}U}{\text{d}T}\right],\ i=a,c \tag{8}$$

$$k_{\text{Li}}(T) = k_{\text{t298,15}i}\, e^{-\text{E}_{\text{ak},i}/R}\left(\frac{1}{T} - \frac{1}{298.15}\right),\ i=a,c \tag{9}$$

$$D_{\text{Li}}(T) = D_{\text{t298,15}i}\, e^{-\text{E}_{\text{ad},i}/R}\left(\frac{1}{T} - \frac{1}{298.15}\right),\ i=a,c \tag{10}$$

with the parameters $E_{\text{ad},i}$ and $E_{\text{ak},i}$, which represent the activation energy for diffusion and the activation energy for reaction of electrodes, respectively.

Regarding separator/electrolyte and liquid phase of both electrodes (anode and cathode), the diffusion coefficient as a function of temperature, $D_i(T)$, is established by Equation (11):

$$D_{\text{Li}}(T) = 10^{\left(-(0.22c)-4.43-\left(\left(\frac{54}{T-229-5c}\right)\right)\right),\ i=a,s,c} \tag{11}$$

where $c$ is the concentration of lithium-ion.

Finally, all boundaries between the battery and the external environment, the heat flux transfer between the battery and the external environment, is described by Equation (12):

$$-\lambda_i \nabla T = h(T_{\text{external}} - T),\ i=a,s,c \tag{12}$$

where $h$ is the heat transfer coefficient.

In recent years, with the replacement of the typical liquid electrolyte with a solid electrolyte, a new type of battery designated solid-state lithium-ion batteries appears. The investigation of this type of lithium-ion battery has been increasing. Then, the main electrochemical equations that govern the phenomena of solid-state lithium-ion battery[9] will be presented.

Regarding the separator with the presence of a solid electrolyte, the transport of lithium-ions ($Li^+$) and negative ions ($n^-$) is described by the Nernst-Planck equation, as shown in Equation (13):

$$N_i = -D_i \,.\, \nabla c_i + \left(\frac{z_i \,.\, F}{R \,.\, T}\right) D \,.\, c_i \,.\, \nabla\varphi_{\text{E}},\ i = \text{Li}^+, n^- \tag{13}$$

where $D_i$ is the diffusion coefficient of ions (negative and positive) and $z_i$ is charge of ions.

In the solid electrolyte occurs the ionization reaction which causes the presence of mobile Li-ions and uncompensated negative charges ($n^-$). The dissociation rate for this reaction is designated by $k_{\text{diss}}$, and the recombination reaction rate by $k_{\text{rec}}$. In this context, lithium-ion recombination/dissociation rate is described by Equation (14):

$$r_{\text{Li}^+} = k_{\text{diss}}\left(c_{0,\text{Li}^+} - c_{\text{Li}^+}\right) - k_{\text{rec}}\left(c_{\text{Li}^+}\right)c_{n^-} \tag{14}$$

where $c_{\text{Li}+}$ an $c_{\text{n}}$- are concentration of lithium-ion and concentration of negative ion, respectively.

The relation between the dissociation reaction rate ($k_{\text{diss}}$) with recombination reaction rate ($k_{\text{rec}}$) is shown in the following Equation (15):

$$r_{\text{Li}^+} = k_{\text{diss}}\left(c_{0,\text{Li}^+} - c_{\text{Li}^+}\right) - k_{\text{rec}}\left(c_{\text{Li}^+}\right)c_{n^-} \tag{15}$$

Equation (16) shows the fraction of total lithium dissociated at equilibrium, $\delta$:

$$c_{Li^+}^{\text{Eq}} = c_{n^-}^{\text{Eq}} = \delta c_0 \tag{16}$$

Within the scope of electrodes, the transport of solid lithium through the positive electrolyte (Fick's law) is described by the following Equation (17):

$$N_{\text{Li}} = -D_{Li,\text{solid}} \,.\, \nabla c_{\text{Li}} \tag{17}$$

where $D_{\text{Li, solid}}$ is the diffusion coefficient for solid lithium through the electrolyte at positive electrode.

At the electrode/electrolyte interface, the kinetics reactions at the negative electrode (Equation (18)) and positive electrode (Equations (19) and (20)) described by the Butler–Volmer kinetics equations are:

$$i_{neg} = F \,.\, k_{neg}\left(\frac{c_{Li^+}}{c_{0,Li^+}}\right)^{\alpha_{neg}}\left(e^{(\alpha_{neg}Fn)/RT} + e^{-((1-\alpha_{neg})Fn)/RT}\right) \tag{18}$$

$$i_{\text{c}} = i_{0,c}\left(e^{(\alpha_c Fn)/RT} + e^{-((1-\alpha_c)Fn)/RT}\right) \tag{19}$$

$$i_{0,c} = Fk_c\left(\frac{(c_{\text{Li,max}} - c_{\text{Li}}).c_{\text{Li}^+}}{(c_{\text{Li,max}} - c_{\text{Li,min}}).c_{0,\,Li^+}}\right)^{\alpha_c}\left(\frac{(c_{\text{Li}} - c_{\text{Li,min}})}{(c_{\text{Li,max}} - c_{\text{Li,min}})}\right)1-\alpha_c \tag{20}$$

where $c_{\text{Li,max}}$ and $c_{\text{Li,min}}$ are the maximum and minimum concentrations of lithium in the solid electrode, respectively. Finally, the overpotential, $\eta$, is defined by Equation (21):

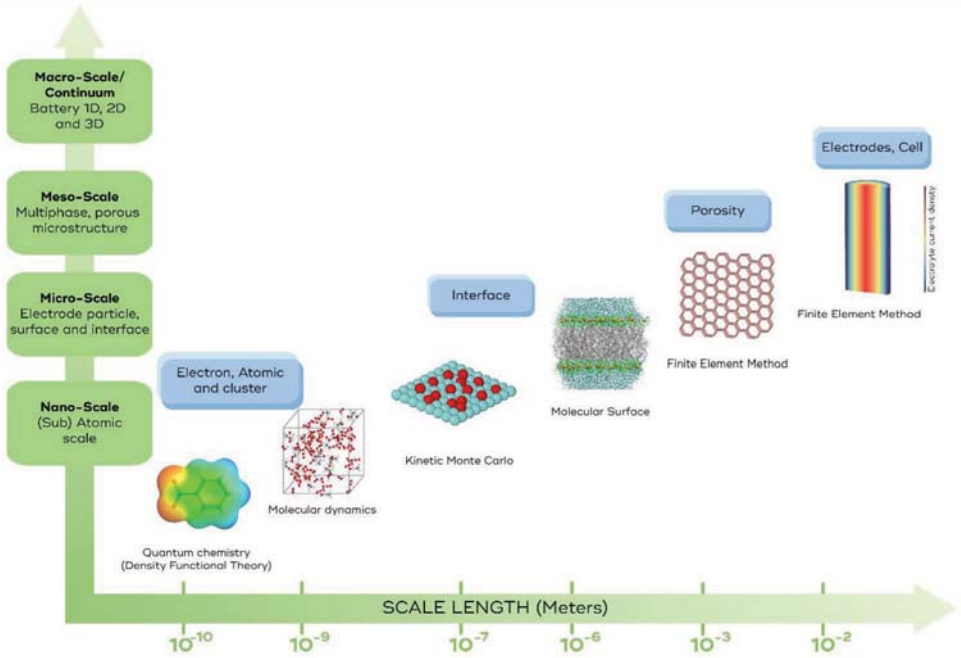


**Figure 3.** Different physical-chemical scales in the modeling of battery materials and battery operation.

$$\eta = \varphi_0 - \varphi_E - E_{eq,i} \quad (21)$$

with the parameters $E_{eq,i}$, $\varphi_E$ and $\varphi_L$, which represent the equilibrium potential in the electrode, the potential of the electrodes and electrolyte, respectively.

### 2.1. Theoretical Modeling of Lithium-Ion Batteries

Modeling of battery components, processes, and materials have been studied at different physical-chemical scales. Different physical levels—molecular scale, nanoscale, microscale, mesoscale, and macroscale—of the batteries operation, which are studied with different models and theoretical approaches, are presented in **Figure 3**.[10]

Theoretical models are based on equations that reflect the physical and electrochemical principles that govern the different processes and phenomena that define the performance and life cycle of lithium-ion batteries. Computer simulation methods have encompassed a wide range of spatial and temporal scales as represented in Figure 3.

Multiscale calculation methods, microscale methods (first-principles (FP) calculations,[11] molecular dynamics (MD),[12] quantum mechanics (QM),[13] and Monte Carlo (MC)[14]), mesoscale (phase-field (PF) method,[15] and force-field (FF) approach),[16] and macroscale approaches (Finite Element Methods (FEM)[5c]) have been applied in the area of rechargeable lithium-ion batteries.

With the development of computational efficiency, simulations based on density functional (DFT) theory and MD have been applied to predict molecular interaction,[17] interfacial reactions,[18] ion transport mechanisms,[19] and to study material properties to improve battery performance, leading to the development of material databases. Some of these databases are: Cambridge Structural Database,[20] Inorganic Crystal Structure Data-base (ICDS),[21] Open Quantum Materials Database,[22] and Materials Project database,[23] among others.

However, with the investigation of more complex materials, theoretical studies of DFT and MD become ineffective due to the high computational demand,[24] and the enormous obstacles that DFT and MD face with the increase in system size and necessary precision. The lag between the results obtained in the simplified theoretical models and the reality makes it difficult to apply computer simulations to describe the complex interface processes that occur in batteries, such as the solid electrolyte interface (SEI) formation, thermodynamics and kinetics of internal reactions, ionic transport behavior at liquid-solid or solid-solid interfaces, among others.

Computer simulations, when resorting to simplified theoretical models in order to lower the computational cost, often neglect a high amount of data on battery materials available in databases.[25] In this context, with the emergence of Artificial Intelligence (AI), more specifically the branch of Machine Learning (ML), new opportunities arise within the scope of theoretical and experimental studies in the area of lithium-ion battery development.[26] Compared to the traditional one-by-one approach, high-throughput technologies can generate a large and high-quality database in a short time at low cost. The design, selection, and integration of materials determined by ML also demonstrate to be a suitable approach with relevant contributions also in relation to other simulation technologies. ML technologies allow exploring new resources for DFT calculations and new potentials for MD simulations, significantly improving the study of phenomena that occur at amorphous and complex interfaces and structures. ML has a high potential to explore and reveal valuable information from experimental and theoretical data sets, improving prediction in the behavior of ionic conductivity, solid–solid interfaces,

liquid–solid interfaces, and battery life, as well as allowing to optimize and accelerate research procedures in the area of Li-ion batteries. Further, ML may facilitate the combination of multiscale simulations.[27]

ML statistically interprets data contained in a database to produce reliable and repeatable decisions and results.[28] Generally, any ML-based approach starts with building an adequate and complete dataset. Subsequently, the ML model must be trained and evaluated for accuracy. In the most common case, supervised methods are obtained using a portion of the dataset to train the algorithm (training stage), where the predictive ability is evaluated by comparing the values predicted by the method and the remaining data that were not used in the training stage, being designated as the test stage.

After obtaining the ideal model, the supervised ML algorithm will be used to predict the results.[29] ML algorithms are classified as supervised learning, unsupervised learning, or reinforcement learning methods.[30] Supervised learning methods use pre-treated data sets to define certain variables as inputs and others as outputs. This procedure does not occur in the case of unsupervised learning ML algorithms, whose objective is to find patterns in the dataset. In ML-supervised learning, it is possible to achieve regression and classification, where a classification is an ML approach that analyzes the dataset into classes, while regression analyzes the data as continuous values.[29]

In ML supervised learning, the classes used can be obtained from ML unsupervised learning. **Figure 4** shows the ML algorithms used in supervised learning, unsupervised learning, and reinforcement learning methods applied in lithium-ion battery research.

Some ML algorithms applied in lithium-ion battery research to obtain predictive models include:[29] artificial neural network (ANN), Decision Tree (DT), Random Forest (RF), Boosting and Bagging Approaches, Support Vector Machine (SVM), U-Net, k-Nearest neighbors (kNN), Naive Bayes (NB) Classification, Generative Models and Inverse Design (class of unsupervised ML algorithms), K-Means and Gaussian Mixture.

Briefly, in the first step, data can be collected from existing databases resulting from experimental measurements and/or theoretically obtained values from computer simulations. Then, the data are submitted to the process of data cleaning and data engineering (Feature Engineering) which is based on the extraction and selection of data. Briefly, the original data can be converted into samples to train the ML model; the mapping relationship between the conditional attributes and the decision attributes can be simulated by selecting the appropriate and optimal ML algorithm. Finally, the models obtained from the ML will allow to be explored with the aim of predicting new results for the development of rechargeable batteries.

In many cases, there is an interaction between conventional theoretical simulations (DFT, MD, and FEM) with ML methods. DFT/MD-assisted ML methods have been developed that contribute to DFT/MD-based predictions. FEM-assisted ML prediction methods have been applied, showing great predictive potential, however, FEM-assisted ML is still in the implementation phase, a path still to be explored.[31] It is important to emphasize the fundamental role of the interaction and contribution of all current three workflow cycles: experimental discovery cycle for batteries, computation model cycle, and ML learning cycle (**Figure 5**). These three work cycles should synergistically interact with each other in order to improve the overall battery research.

In the development of studies to predict and optimize the performance of lithium-ion batteries, the ML Cycle, the Computational Model Cycle, and the Experimental Discovery Cycle domains interact with each other, as represented in Figure 5. The results obtained in the experimental battery domain and in computational simulation (FEM, DFT, among others) are introduced in databases that will be used in ML. After the implementation of the learning algorithm, new predictions and optimization results are obtained that will be validated through the experimental component, leading to an improvement of the empirical knowledge for the development of new prototypes. Further, experimentally obtained results allow to validate the models developed in the field of Computational Simulation which in turn will also produce theoretical results to understand and guide the Experimental Design and the development of advanced materials and prototypes.

The combination of databases and ML approach has been applied to design and predict material properties of electrodes, including crystallinity, chemical stability, and voltage, from the atomic scale to mesoscale. Bearing this in mind, ML can be applied to design new solid-state electrolytes (organic and

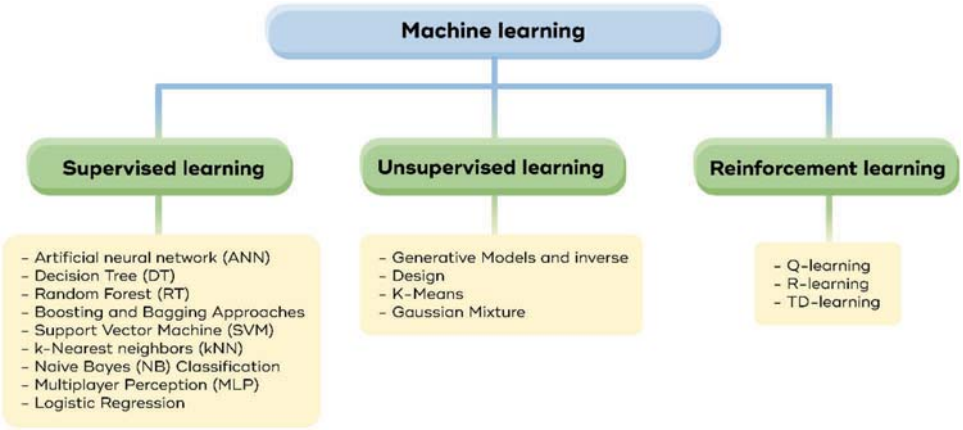


**Figure 4.** Schematic representation of ML methods and algorithms.

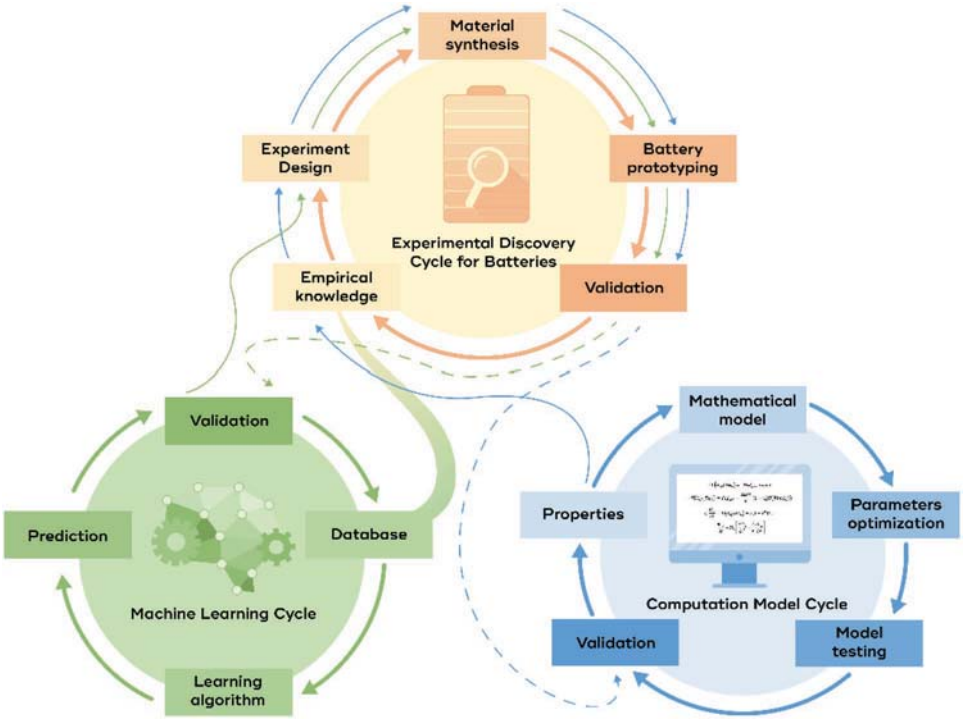


**Figure 5.** The three workflow cycles of battery research: experimental discovery cycle for batteries, computation model cycle, and ML learning cycle.

inorganic) with fast Li-ion transport and mechanical properties, providing an opportunity for exploring material properties at a lower cost and accelerating the material discovery processes.

There are an increasing number of works based on the applications of ML in battery research, essentially with respect to the characterization and discovery of new materials with predicted specific properties. The discovery and optimization of materials applied to batteries have been a powerful tool for analyzing experimental and theoretical data and, from them, extracting the relationships between their structures and functional properties, with a wide range of review articles addressing this topic.[27,32]

ML methods have been applied to predict and develop materials for rechargeable battery electrodes, solid electrolytes, and liquid electrolytes.

For the electrode dimensions and structure, ML simulations have been performed to find optimal designs that allow highest possible combination of capacity and power output. For improving power performance, a homogeneous electrochemical activity between the electrodes in the 3D design is essential. In the case of materials for battery electrodes, ML methods have been applied to predict voltage profiles of a wide range of active materials for Li-, Mg-, Ca-, Al-, and Zn-ion batteries through the implementation of different algorithms.[33] About 5000 electrode materials were proposed to be used in sodium and potassium ion batteries based on voltage profile diagrams and comparing them to the DFT calculations (a website was developed for the estimation of the voltage of electrode materials).[34] Research has been also performed for the design of new organic materials for electrodes based on the prediction of quantum mechanical quantities (redox potentials) and electronic properties (electron affinity, lowest unoccupied molecular orbital (LUMO), highest occupied molecular orbital (HOMO)) through artificial neural networks using the quasi-Newton method.[35] Calculations of lattice constants for fully lithiated and delithiated structures have been also performed to design low-strain cathode materials, based on ML models combining ab initio calculations and partial least squares (PLS) analysis with the Quantitative Structure–Activity Relationship (QSAR) formulations, allowing to predict the percentage change in volume of spinel and layered-type oxides (**Figure 6**a).[36] Further, significant achievements have been presented in predictive studies related to crystalline cathode systems,[37] the configuration energy of $LiNiO_2$ (LNO) and $LiNi_{0.8}Co_{0.15}Al_{0.05}O_2$ (NCA) cathodes,[38] the redox potentials of electrodes,[35] and to the impact of manufacturing parameters on the final characteristics of the electrodes (porosity and mass loading).[39] Takagishi et al.[40] used ANN simulations to predict the charge/discharge specific resistance in porous structures by analyzing the effects of porosity, components volume fraction, calendering process, and electrolyte compatibility parameters in the electrode preparation. It was observed that the packing process should be around 50%, that small active material particles are more suitable, and that their volume fraction should be between 0.5 and 0.8. 3D U-Net architecture simulation was used to create an accurate 3D LIB electrode image taking into account the electrode particles (active particles and binder) and the pore phases. The originated database and further improvement of this database by the scientific community will allow to further improve electrodes.[41]

ML simulation have been applied to study the separator structures of LIBs. The prediction of the mechanical behavior of the separators was studied by combining FEA and ML strategies. The proposed method shows that applying a unidirectional force during mechanical stress allows to predict the growth of

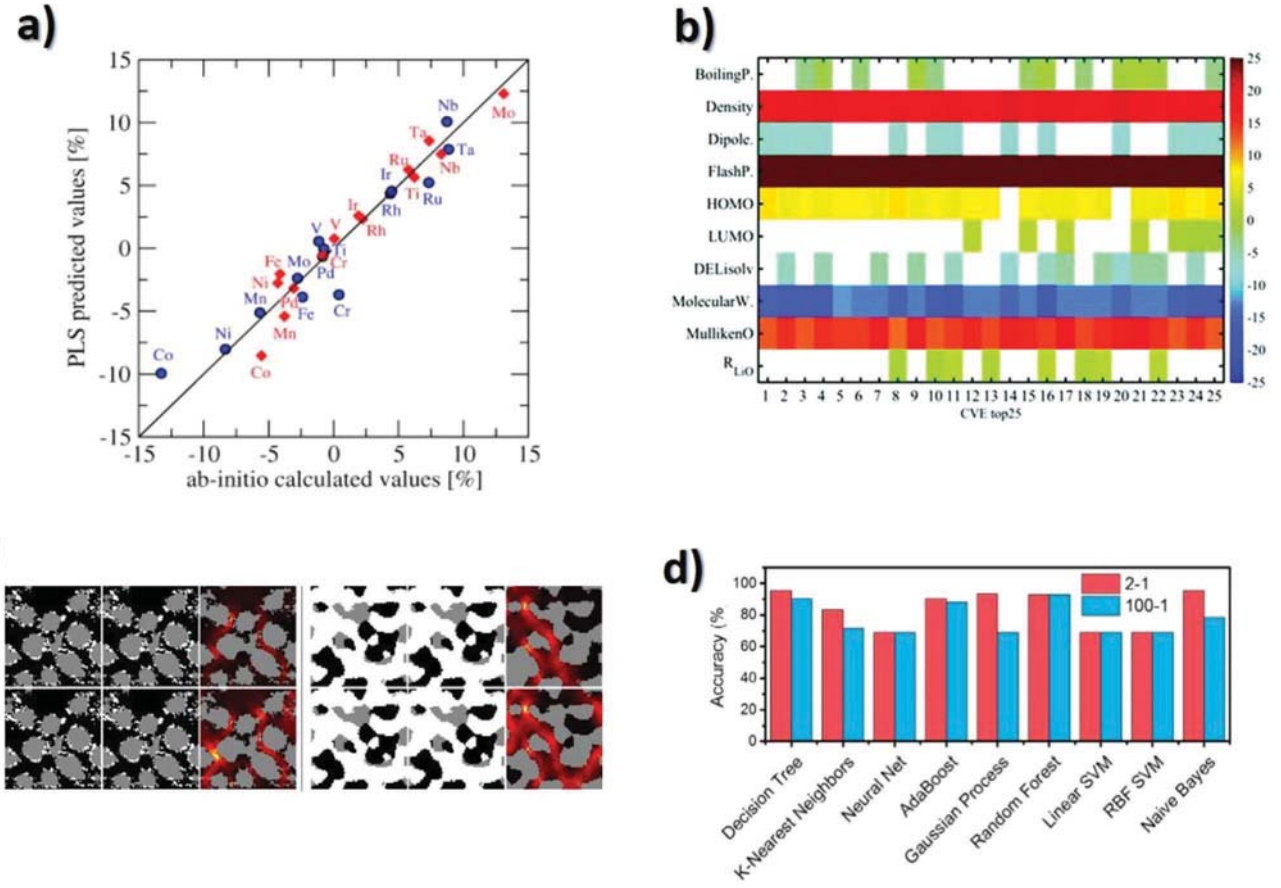


**Figure 6.** a) Predicted cathode volume changes for partial least squares as a function of ab initio-derived, where the data from $LiX_2O_4$ spinel is represented by blue circles and $LiXO_2$ layer structure by red diamonds. Reproduced with permission.[36] Copyright 2017, Elsevier. b) Weight diagram of descriptors obtained from the top 25 combinations of descriptors, for the melting point prediction. Reproduced under the terms of the CC BY 3.0 license.[44] Copyright 2018, The authors, published by Royal society of chemistry. c) Periodic microstructure generated for Li-ion cathode (left) and SOFC anode (right) with flux maps generated from steady-state diffusion simulations in TauFactor. Reproduced under the terms of the CC BY license.[50] Copyright 2020, The authors, published by Springer Nature. d) Prediction accuracy comparison between the different ML algorithms calculated from the same data. Reproduced with permission.[52] Copyright 2019, John Wiley and Sons.

the voids, important to understand the failure mechanism of thermal runaway of the battery when subjected to an external force.[42] ML has been also applied to the optical inspection of the separators, preventing in this way structure defects. The objective is to distinguish between defect classes as non-quality optical effects and faults.[43]

Within the scope of the development of liquid and solid electrolytes, studies have been increasingly carried out with the application of ML methods in order to predict coordination energies and melting temperatures of solvent molecules (Figure 6b),[44] predict the diffusion barrier of lithium ions from a set of compositions,[45] prediction of the ionic conductivity of nanocomposite polymer electrolyte systems (PEO-$LiPF_6$-EC-CNT),[46] prediction of the transport characteristics of lithium-ions and identification of the descriptors that are responsible for the high conductivity of lithium-ions in garnet-structured oxides,[47] evaluation of possible reactions and thermodynamic stability of $Li|Li_7La_3Zr_2O_{12}$ (LLZOM, M = dopant) interfaces under various chemical conditions,[48] prediction of the low-temperature ionic conductivity of a large variety (72) of compounds,[49] reproduction of 3D electrode structures (Figure 6c),[50] and effect of electrolyte channel geometrical parameters,[51] among others.

With respect to overall battery performance, ML methods have been applied to predict the lifespan of batteries and to monitor the state of health of lithium-ion batteries, accurately predicting the state of charge (SOC), state of health (SOH), and remaining useful life (RUL) parameters and allowing to implement intelligent battery management system (BMs). As an example, a set of ML algorithms such as DT have been implemented to analyze battery lifespan (Figure 6d).[52] A powerful ML-based tool has been also proposed to develop safety envelopes for lithium-ion pouch battery cells.[53] Regarding the prediction of battery performance, a model based on the Extreme Learning Machine (ELM) method was proposed to predict the evolution of battery temperature, voltage, and power.[54] Further, some studies have faced the challenge of developing linear models that accurately predict the cycle life of commercial lithium iron phosphate (LFP)/graphite cells.[55] Also, a multikernel support vector machine (MSVM) model based on polynomial and radial kernel functions was proposed to predict the battery remaining useful life (RUL).[56] In order to obtain more

accurate diagnoses of the state of the batteries, ML methods have been applied to obtain accurate predictions and monitoring of the SOC, SOH, and RUL parameters of lithium-ion batteries.[57]

FEM-assisted ML is still in the implementation phase and the main objective is the prediction of the operation of the batteries. Thus, the computational simulation of energy storage systems will allow to predict battery performance before assembling the prototypes in a laboratory environment, reducing costs in terms of material and time.

The first electrochemical model was proposed[58] in the 90's by Doyle/Fuller/Newman and describes the physicochemical phenomena that occur during the charge/discharge behavior of a battery (equations provided in Table 1). From its original proposal, this model has been modified by several authors to include in detail all the processes that describe battery operation, taking into account the innovations in materials and the understanding of specific effects, such as the ones at the interfaces. The model is based on ordinary and partial differential equations, and the FEM is one of the most used methods for its numerical resolution. In addition, its resolution has been optimized through computational efficiency.[10b]

During the development steps of computer simulations, it is essential to define the dimension of the lithium-ion battery model (1D, 2D, or 3D) to be applied, as shown in **Figure 7**. The selection of the model dimension will depend on the study that is intended to be implemented, as well as the optimization of computational efficiency.

When it is only intended to evaluate and measure the gradients of the physical and electrochemical variables along the cartesian axis of xx, the 1D model of the battery is implemented. The battery components (electrodes, separator, and current collectors) are represented by a line, as shown in Figure 7a. As demonstrated in Figure 7b, when 2D models of the batteries are applied, the respective components are represented by planes and the gradients of the physical and electrochemical variables along two cartesian axis (xx and yy axis) will be measured. In the 3D battery representation, its components are represented by volumes, allowing the measurement of the gradients of physical and electrochemical variables in the three Cartesian axis (xx, yy, and zz axis), as shown in Figure 7c. In summary, the battery model dimension will be implemented considering the optimization study which is intended to be carried out and the cost / computational resources associated with computational efficiency.[10b]

### 2.2. Computer Simulations Applied to Lithium-Ion Batteries at the Macro and Micro-Scales

As described in the previous subchapter, the Doyle/Fuller/Newman electrochemical model[58] was the first theoretical model to describe battery operation, being nowadays still the main model used in the field. It includes a large variety of relevant parameters, allowing a large diversity of simulations, as shown in **Figure 8**, depending on the main purpose of the specific simulation. Figure 8 also shows some of the most relevant simulation parameters, including geometrical ones, electrode-specific characteristics, or separator/electrolytes, among others.

The theoretical models have been developed as a consequence of the need to evaluate different materials for the different battery components (active materials, polymers, and electrolytes). Further, the influence of battery geometry on its performance and the study of the thermal, mechanical, and

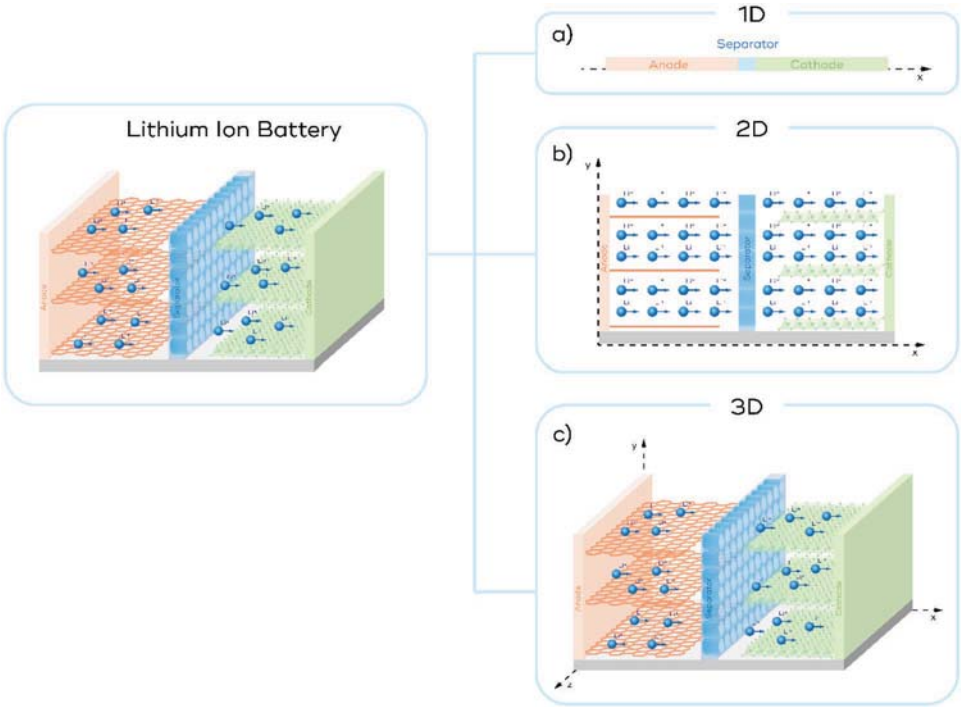


**Figure 7.** Representation of the a) 1D, b) 2D, and c) 3D battery model dimensions.

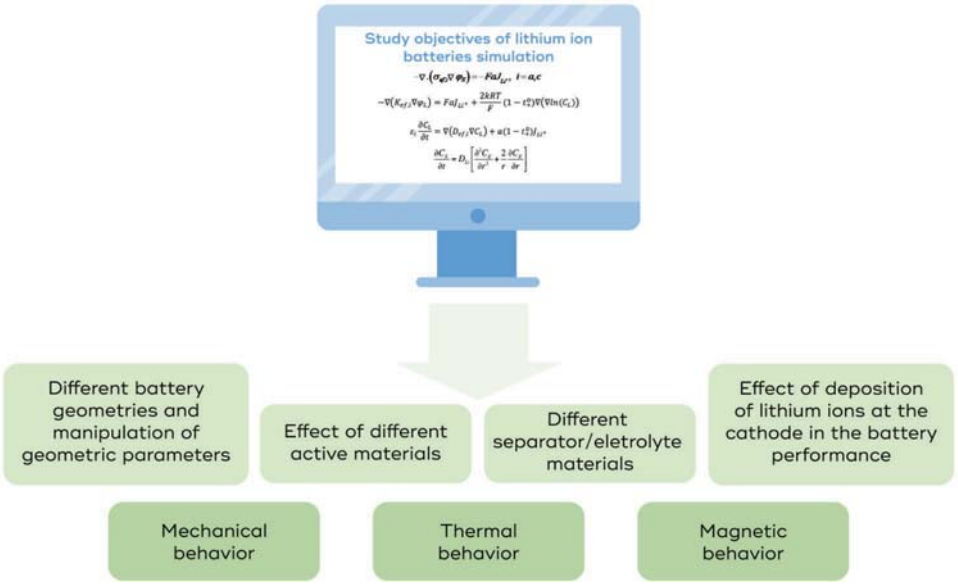


**Figure 8.** Effects that have been evaluated through the theoretical simulation of lithium-ion batteries.

magnetic behavior of a battery has been explored throughout its operating process. After the development of the Doyle/Fuller/Newman electrochemical model, a large number of simulation studies were developed. Thus, the deposition of lithium ions at the cathode was studied using different geometries (length of the electrolyte with respect to the electrodes and the length of the cathode with respect to the anode), demonstrating the impact of the concentration gradients of lithium within electrodes on electrolytic current distributions, that in turn depend on the cell charge level[59] The influence of the electrodes and separator dimensions in the generation of overpotential at the electrode edges was demonstrated,[60] as well as the effect of the porosity of the electrodes[7] and the separator on battery performance, the latter being optimized for a degree of porosity above 50%.[61] The effect of active material particle size on the performance and degradation of batteries was addressed, showing that the main effect of larger particles is to lead to longer diffusion paths.[62] The porosity of the electrodes also influences the capacity fade in lithium-ion batteries, based on its effect on both reversible intercalation processes and irreversible parasitic reaction.[63] The pore structure of the electrodes also leads to variations of the local tortuosity and Bruggeman coefficient, which in turn leads to variations in the mass transfer.[64,65] A better understanding of the effect of ion conduction and diffusion phenomena in the electrodes[66] and in the separators[65,67] on battery performance has been achieved allowing the determination of the best geometries for the different battery components. Studies also have focus on the relevant issue of electrolyte deterioration, for example in Li-air batteries, which leads to a decrease of the discharge capacity as a function of cycle number due to the irreversible formation of $Li_2CO_3$ discharge products.[68] Finally, the calculation of discharge overpotential distributions allows to analyze the contributors to resistance in the anode, cathode, and separator regions, as a function of thickness increase, showing that the main overpotential contribution shift from interfacial to ionic, with both originating from the electrodes.[69]

With respect to the influence of materials characteristics on the performance of the different battery components (electrodes, separator, and electrolyte), different porous active materials have been used for the electrodes[64b,66e,70] and different polymer materials,[71] separator thickness,[72] electrolytes of different chemical nature,[66a] and lithium-ion concentrations within the electrolytes[7] for the separators. Also, a large relevance has been attributed to the influence of the battery geometry on its performance. In particular, the simulation of different battery geometries contributed to a performance increase at different discharge rates,[73] the interdigitated geometry being the most studied geometric configuration.[74]

With the emergence and increasing implementation of lithium-ion batteries for electric and hybrid vehicles and energy harvesting systems, simulations have been performed at different thermal conditions, mechanical pressures, and external magnetic fields. The electrochemical model coupled to the thermal model allowed to study the influence of different thermal conditions on battery performance,[8a,d] evaluating the different sources of heat produced by the batteries along their charge and discharge processes,[75] as well as the evolution of internal temperature and battery capacity when subjected to different external temperatures.[76] The optimization of the battery geometry allowed for improving the heat dissipation efficiency and controlling the temperatures reached by the battery during its charging and discharging processes, evaluating its impact on the degradation of the materials of its components.[77] Mechanical models have been used to study the battery performance when subjected to external mechanical pressures.[78] Likewise, internal mechanical pressure values generated by the battery during its operating cycles[79] were obtained. Recently, studies have emerged on the influence of external magnetic fields on battery performance.[80]

Furthermore, in order to replace conventional liquid electrolytes with solid polymer electrolytes (SPEs), computer simulations play an important role to reach the next generation of more efficient and safer solid-state lithium-ion batteries.[9]

## 3. Battery Separators: Main Role and Relevant Properties

An important component in battery devices is the separator, placed between electrodes, and for lithium-ion batteries, acts as the lithium-ion transfer medium between the electrodes, while providing mechanical stability, thermal resistance, and avoiding short-circuit of the battery.[81] There are different types of separators, including microporous membranes, nonwoven films, electrospun membranes, membrane with surface modifications, composites, and polymer blends.[82]

The most used separators rely on a porous membrane wetted by an electrolyte solution,[67] which consists of non-aqueous solvents with high dielectric constant ($\varepsilon$), low viscosity ($\eta$) and that are in a liquid state in the battery temperature range.[83] **Figure 9** shows the main characteristics of the separator divided by structural and chemical.

The thermal stability of the separator is critical for the migration of ions in LIBs and to keep stable the separator morphology, as dimensional variations by compression decrease the ion transport channels and their migration, decreasing the value of the discharge capacity.[84]

Separators are typically manufactured based on polymer materials, the most used being polyethylene (PE), polypropylene (PP), polyvinyl chloride (PVC)), and polyvinylidene fluoride (PVDF) and co-polymers and different processing techniques such as wet processes and dry processes such as extrusion,[85] electrospinning,[86] nonwoven techniques,[87] atomic layer deposition,[88] solvent casting with thermally induced phase separation,[89] and non-solvent phase separation processes (NIPS),[90] among others[91] where its surface can be modified by plasma treatment.[92] The thickness of the separators typically varies between 25 and 40 µm, depending on the type of battery, they show a degree of porosity larger than 40%

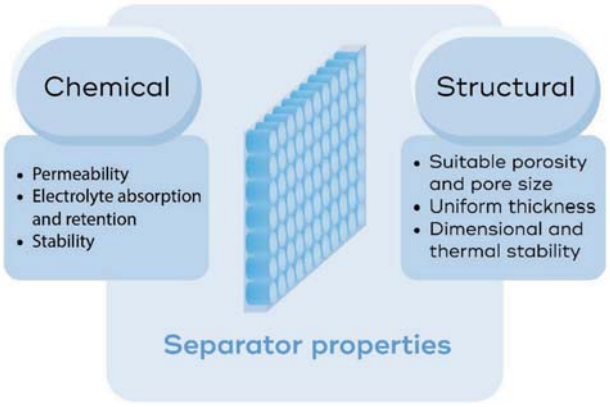


**Figure 9.** Main characteristics of the battery separators for lithium-ion batteries.

with an average pore size below 1 µm and are stable at temperatures up to 150 °C. Additionally, to improve the thermal and mechanical properties and wettability of the conventional separators based on PE and PP, new separators based on covalent organic framework (COF) into poly(arylene ether benzimidazole) (OPBI),[93] polyacrylonitrile (PAN) composite separators with cellulose acetate and nano-hydroxyapatite,[94] PAN with aluminum diethylphosphinate (ADEP),[95] polyimide (PI) polymer,[96] PI with polyethylene oxide (PEO) processed by electrospinning technique,[97] PI with zirconia ($ZrO_2$),[98] PI with graphene,[99] PI with hexagonal boron nitride,[100] PI with nano-ti$O_2$,[101] PI with organic montmorillonite (OMMT),[102] PEO with para-aramid nanofibers (ANFs),[103] PVDF/$SiO_2$,[104] poly(ethylene glycol) diacrylate (PEGDA),[105] polyurethane separator coated $Al_2O_3$ particles,[89a] and poly(vinyl alcohol) with nano architecture halloysite nanotubes (NHNTs) composite separator (OPVA/NHNTs separator,[106] and new coatings of boehmite ($\gamma$-AlO(OH)) nanofibers,[107] inorganic oxide solid electrolyte layers ($Li_{1.3}Al_{0.3}Ti_{1.7}(PO_4)_3$, LATP),[108] $SiO_2$ with acrylamide (AM),[81a] $Ca_3(PO_4)_2$ inorganic layer,[91] polyimide microsphere,[109] and plasma treatment plus zwitterion grafting[110] were developed. Further, it has been also explored the replacement of these synthetic polymers by natural polymers such as, natural wood,[111] cellulose,[96,112] silk fibroin,[113] silk fibroin with sericin,[114] poly(vinyl alcohol) (PVA),[115] lignin,[116] carrageenan,[117] among others.

Furthermore, the development of different separators allowing to restrain of Li dendrite growth, such as, graphene oxide onto electrospun polyacrylonitrile (HGO-PAN) (**Figure 10**a).[118] In this work, Li dendrite retain were verified experimental and theoretically by FEA simulation, where the electrostatic field and Li-ion transport were simulated (by Nernst-Einstein equation) and confirmed a uniform distribution of Li-ion flow due to the HGO layer.

An important and widely used separator type relies on composites that consist of different filler types, such as, inert ceramic and super acid oxides,[119] clays (MMT),[120] molecular sieves,[121] zeolites,[122] and metal–organic frameworks (MOFs),[123] among others[124] into the different polymer matrix[82b,109] as well as polymer blends (Figure 10b) which are the combination of two and/or more different polymers to tailor specific properties of the separators: wettability, flame retardancy, mechanical properties, and ionic conductivity, among others.[82b,c,125] Currently, one of the most explored fillers in composites is MOFs as they add flame-retardant properties to the separator membrane.[82e,126]

Thus, composite separator membranes based on poly(vinylidene fluoride-cohexafluoropropylene) (PVDF-HFP) with different MOFs (MOF-808, UiO-66-$NH_2$, and MIL-125) show that MOFs also promote lithium migration across the separators during the battery operation.[127]

In addition, the conventional electrolyte has been replaced by ionic liquids in order to improve battery safety, as in the separator electrospun membranes of polyhedral oligomeric silsesquioxane (POSS)/polyvinylidene fluoride (PVDF).[127] As previously mentioned, the separator plays an important role in the overall battery performance, with simulation studies being required both at the structural and chemical levels.

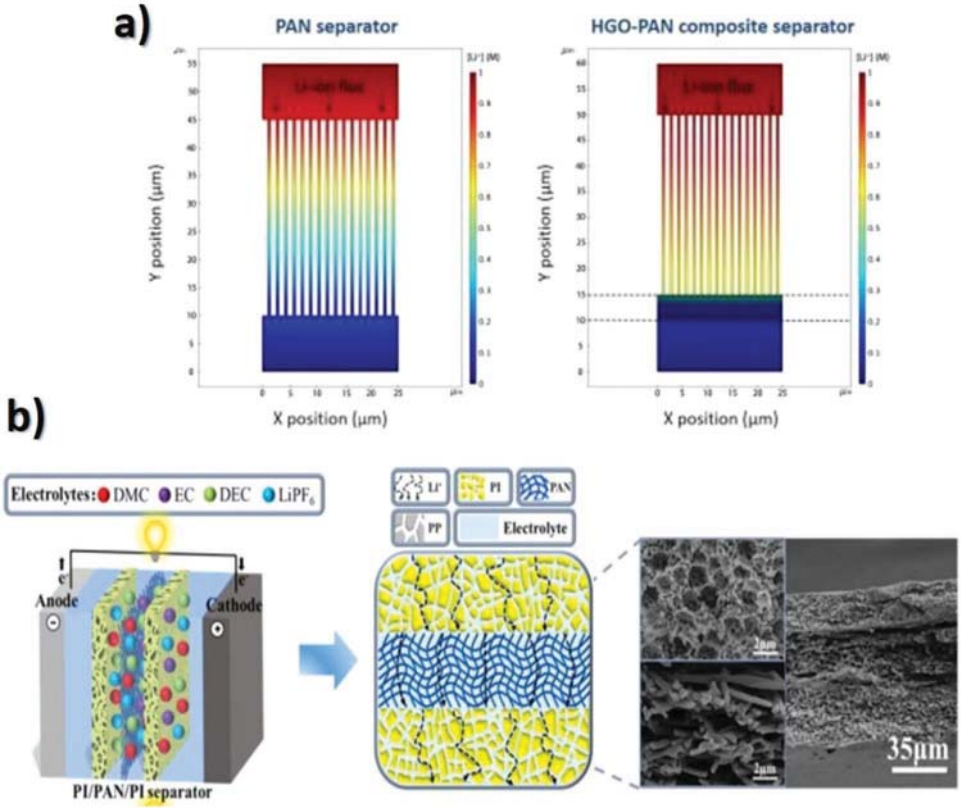


**Figure 10.** a) Simulation study of $Li^+$ distributions through PAN separator and HGO-PAN composite separator. Reproduced with permission.[118] Copyright 2022, Elsevier. b) Electrolyte state and lithium-ion transport paths with the corresponding SEM images for a PI/PAN/PI separator. Reproduced with permission.[125] Copyright 2022, Elsevier.

### 3.1. Theoretical Simulation of Battery Separators

The simulation of the main properties of battery separators has been typically performed at a structural (macro-scale) and chemical (lithium-transport time scale in seconds). MD has been widely used to study the different types of electrolytes in order to evaluate the solvation process, strongly dependent on both the salt and solvent, the $Li^+$ diffusion, and the existing chemical reactions[128] as well as on the thermal properties linked to the ionic transport.[129] Furthermore, molecular scale simulations have been also performed with different electrolyte solvents such as ethylene carbonate (EC), dimethyl carbonate (DMC), and EC+DMC for cellulose lignin separator structure. It was verified that lignin positively affects the separator structure probably due to new hydrogen bonds created between cellulose and lignin molecules.[130] MD simulation on polyacrylic acid (PAA) has shown that the thermal conductivity of the separator increases with increasing polymer chain length elongation.[131] Also, discrete atomistic models at the molecular level, allowed to analyze the microstructure of the separator under different conditions such as in DMC, water, and vacuum, where the mechanical response depends on the interaction of the amorphous phase with the solvent. It was observed that the DMC solvent decreases the mechanical properties since it can penetrate the amorphous nanofiber against the water solvent which increases Young's modulus through the squeezing of the amorphous phase due to repulsive interactions.[132]

It has been shown that a decrease in electrolyte conductivity is related to changes in the microviscosity of the electrolyte near the separator surface, which restricts the mobility of ions in the separator pores. Thus, the interactions between the ions in the electrolyte solution and the separator membrane can be tailored, as it depends on the structural and chemical properties of the separator.[133] On the other hand, through the FEM simulation, it was demonstrated that the separator surface chemistry interactions with solvent molecules and ions of the electrolyte increase the degree of ion pair dissociation and consequently enable faster ionic transport, increasing the lithium-ion transference numbers.[134]

In the scope of concentrated binary electrolyte within porous separators, ion transport simulations show that long-term relaxation experiments in a two-electrode cell are the most reliable method to determine the concentration.[135]

To study the performance of ionic liquid-based lithium batteries by atomistic simulation, a mathematical model was developed to describe their transport of the ionic components. Mutual diffusion phenomena using Maxwell–Stefan diffusivities allow to describe the transport of lithium ions, leading to a correlation between the porosity and length of the separator, the low rate transport causing a lithium depletion zone in the regions of the porous cathode.[136]

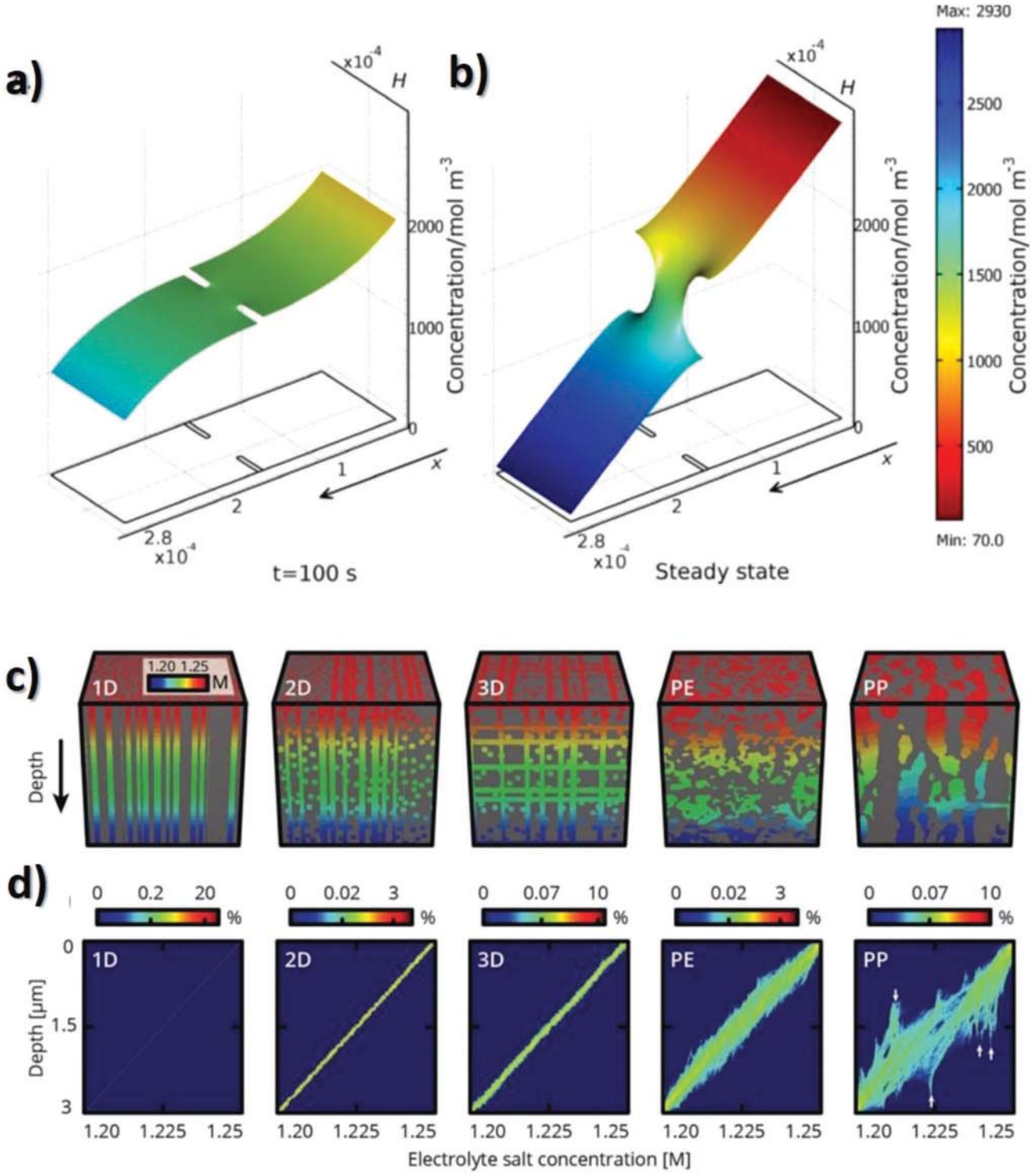


**Figure 11.** Development of the ionic concentration distribution in the electrolyte layer with inserted separator. a) Corresponds to 100 s after applying a constant current, b) corresponds to the steady-state. The applied current is 0.72 A. Reproduced with permission.[137] Copyright 2012, Elsevier. c) Concentration profiles and d) concentration density maps from steady-state Fickian diffusion simulations across the through-plane direction of artificially generated and recorded datasets of 3 µm edge length with a concentration difference of ≈50 mM between top (1.25 M) and bottom (1.20 M). Reproduced with permission.[138] Copyright 2018, Royal society of chemistry.

The ionic transport in Li-ion battery liquid electrolytes (1.5 M $LiPF_6$) within a perforated separator has been studied by a FEM using the Nernst-Planck equation, the concentration gradients in 3D being shown in **Figure 11**a,b, 100 s after the current has been switched on (A) and under steady-state (B) to assess the diffusion and migration overpotentials.[137]

Figure 11a,b shows that $Li^+$ ions start to accumulate at one side of the obstacle, resulting in steep concentration gradients in the vicinity of the pore opening which depends on the pore size. In the perforated separator, the ionic mobility and transport depend on the pore shape.[137]

The electrolyte filling of the separator is a critical parameter to obtain high battery performance and in an experimental and simulation/theoretical work for a polyethylene (PE) separator, it has been observed that it can be up to 30% gas entrapment upon infilling the separator due to its geometry, which results in a reduction of effective transport by > 40%. Furthermore, it was found that the electrolyte properties, such as viscosity, affect the infilling process, with high viscosity leading to high values of trapped gas and consequently decreasing the ionic conductivity value.[139]

Through numerical diffusion simulation, the effect of the topological parameters and node structure of commercial separators (PE and PP) with comparable porosity, tortuosity, and effective transport was evaluated, and the high connectivity of the pores of the PE separators enabling ion gradients at the top of the separator (Figure 11c,d). In this work, it was demonstrated the role of connectivity density for the homogenization of the ion concentration, through the microstructure of the separators.[138]

The optimization of the separator properties by FEM computer simulations is key for optimizing performance. The optimal value of the degree of porosity of a separator has been established to be above 50% and the thickness should range between 1 and 32 μm for improved battery performance independently of scan rate,[61] in order to assure also the mechanical stability of the battery.[140]

Considering that additive manufacturing, photolithography, and replica molding techniques methods allow to achieve different morphologies, the effect of different types of micropatterned separators (arrays of hexagons, lines, zig-zags, and pillars) on battery performance was also evaluated by theoretical simulations through the electrochemical model based on the Newman/Doyle/Fuller equations as shown in **Figure 12**.[141]

It was demonstrated that the high ionic current density of patterned microstructures is attributed to a better diffusion of the ions in the separator channels that affects the ionic conductivity value and lithium-ion transference number.[141]

Furthermore, considering the advantage of patterned microstructures to improve battery performance, separators with tailored pillar diameter, height, and bulk thickness were analyzed by experimental and theoretical simulations using FEM. It was observed that the parameter with the greatest influence on battery performance is the bulk thickness of the separator.[142] The effect of polymer electrolytes into 3D-Microbatteries was evaluated through simulations based on a fully coupled 3D thermal-electrochemical model and it was demonstrated that the separator plays an important role in the associated heat generation. Thus, the higher heat sources appear near the regions with more active charge transfer processes and the generated heat can be mitigated by using a more diffusive electrolyte system that is important for thermal management.[143] Porous anodic aluminum oxide (AAO) has been studied as a separator by computer-aided simulation modeling by FEM method, showing improved performance with respect to electrolyte current pathways when compared with PP separators. This new separator allows to suppress the Li dendrite formation due to the porous framework and low tortuosity, leading to improved battery performance.[144]

Another relevant parameter that affects battery performance is the mechanical properties of the separator. It has been demonstrated by computer simulations based on a macro-scale model in pouch lithium-ion cells that the maximum stress in the separator always emerged at its inner side, when the lithium-ion battery is fully charged, the rest of the separator being in a relatively low and stable stress state. These simulations demonstrate that the local strain and stress in the separator membrane decreased with increasing temperature.[145] The nested finite element ($FE^2$) multiscale framework has been employed to investigate the ionic transport in porous battery cell separators during (dis)charge processes. From the microscale solution, homogenized fluxes and their dependence on the downscaled macroscale variables have been upscaled, demonstrating the drawbacks associated with currently accepted procedures, leading in some cases to severe variations in the prediction of field quantities.[146]

The stress analysis of polymeric separators in a lithium-ion battery was performed using different softwares such as Comsol[147] or LS-Dyna.[148] The simulations with a meso-scale representative volume element (RVE) reveal that the stress in the separator varies in phase with the battery cycles, its state, and magnitude depending upon Young's modulus of the separator, electrode particle size, packing, and the pressure of the cell. Also, it was observed that particles of the electrodes with a loose packing pattern show a tendency to result in tensile stresses in the separator.[147a]

The effect of mechanical stresses arising on SPEs on the electrochemical performance of lithium-ion (Li-ion) solid-state batteries has been studied showing non-uniform ionic concentration profiles developing during the discharge process that induce stresses and deformations within the SPE. Those stresses have been observed to induce ionic redistribution that favors ion transport and increases cell conductivity—up to 15%.[149]

Commercial separators are based on polyethylene (PE) and polypropylene (PP) materials and in this experimental work the effect of compressive deformation on their microstructure was analyzed, showing that deformation affects more negatively PE separators than PP ones. **Figure 13**a shows the ion transport paths remaining connected under compressive loads in both in-plane and in-plane directions for both separator types, being observed that the separator structure has an important role in its mechanical robustness and prevention of battery degradation.[150]

Furthermore, for commercial separators (PE and PP), a 3D microstructure model was developed to predict the mechanical behaviors of the anisotropic battery separator and was used to correlate the experimental and theoretical data obtained by FEM analysis.[152] It has been shown that large strain and pore size in the strain bands can be a potential risk for battery safety issues such as thermal runaway.[152]

Furthermore, the effect of compression on lithium-ion battery separators in different multiscale studies was evaluated at different compression ratios (CRs).

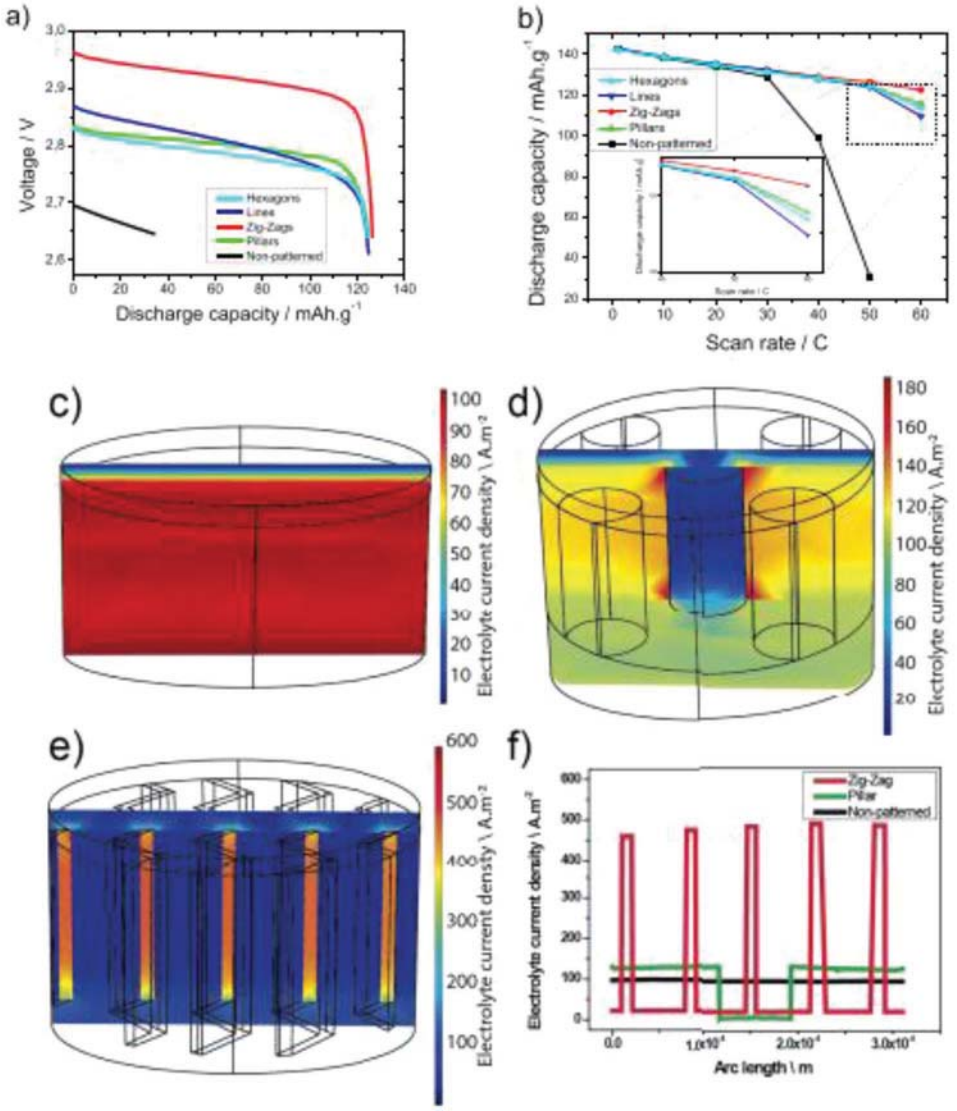


**Figure 12.** Discharge capacity a) for batteries with different separators at 50C-rate and b) for each battery for all C-rates. Color mapping of ionic current density for c) conventional, d) pillar, and e) zig-zag separators. f) Electrolyte current density across a line for each separator. Reproduced with permission.[141] Copyright 2019, Elsevier.

It was observed that the CR affects the mechanical properties and performance of the battery from the microscale to the macroscale. Thus, at CR = 40%, the ionic conductivity decreased by 87.5% leading to a decrease in battery performance.[123b]

High pressure has been also introduced in the electrochemical-mechanical model for studying the compressibility and ionic conductivity of the polyethylene separator. It was shown that the ionic conductivity decreases in the porous structure, the intercalation and deintercalation at the separator interfaces of the electrodes become more accelerated, and therefore, the Li concentration gradient within the electrodes increases with pressure and enhances the Li deposition on the electrode surface during the charging behavior, resulting in the aging process.[153]

Inhibition of lithium dendrites can be also controlled by the separator. The effect of separator pore size in lithium dendrite growth has been evaluated by the phase field method (PFM) and fifth regimes of dendrites growth were verified, as shown in Figure 13b, serving as a guideline to design improved separators. Dendrites growth depends on the separator chemistry, morphology, and transport properties.[151]

The dendrite growth in separators has been also addressed by phase-field simulations as a function of pore size showing that separators with smaller pore sizes are beneficial to smoother electrodeposition.[154] Further, it has been also demonstrated that tortuosity significantly affects the growth rate of dendrites, resulting in a shorter lifetime in the battery. Also, it was observed that the different dendrite growth rates are related to the degree of heterogeneity of the separator with same bulk physical properties.[155]

In addition, a nano-shield (NS) protected separator has been developed by coating $SiO_2$ nanoparticles, the FEM theoretical simulations, and experiments demonstrate that the NS suppresses Li dendrites growth because of the formed narrow

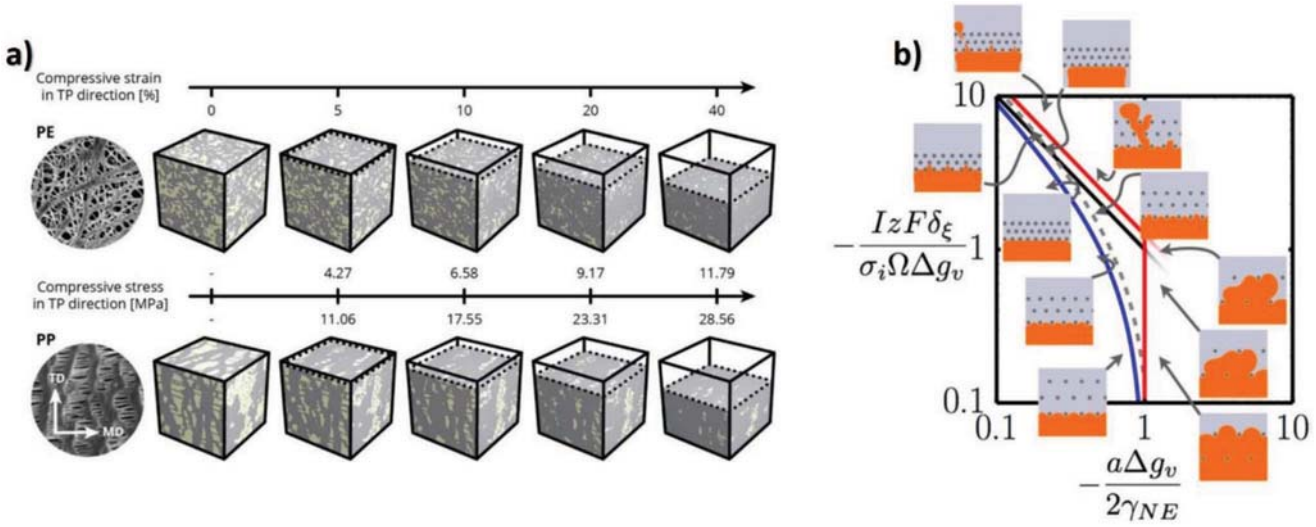


**Figure 13.** a) Top-view scanning electronic microscopy images of 3 µm diameter of isotropic PE and anisotropic PP (with transverse direction, TD, and machining direction, MD) separators. Resulting separator microstructure of electrolyte-immersed PE (top) and PP (bottom) (i.e., gray polymer space and pale-yellow electrolyte-filled pore space) of 3 µm edge length under uniaxial compressive strains of 0%, 5%, 10%, 20%, and 40% in the through plane (TP) direction. The compressive stress in MPa applied to achieve the given percent strain is indicated for each structure. Reproduced under the terms of the creative commons attribution 4.0 license.[150] Copyright 2018, The authors, published by Electrochemical society. b) Predicted regimes of dendrite behavior in a porous separator: the suppression regime, below the blue curve, highlights the loci of pore sizes and recharge rates that are thermodynamically unfavorable for dendrites to grow; the permeable regime, below the black line, where dendrites cannot penetrate more than the very surface of the separator (the first layer of fibers); the penetration regime, between the red and the black line where dendrites rely on electrochemical shielding to find a thermodynamically stable pore to persist inside the separator; and finally, the short-circuit regime, to the right of the red line. Reproduced with permission.[151] Copyright 2015, Elsevier.

channel and mitigates short-circuiting by the reduction of the voltage intensity due to surface effects.[156]

In conclusion, the separator plays an essential role in improving battery performance and its proper selection, design, and interaction with the electrolyte solution provide improved ion transport paths between the electrodes.

## 4. Conclusions

Lithium-ion battery technology has strongly supported modern technology development by powering small portable and electronic devices and, more recently, electric vehicles. Lithium-ion batteries already represent a reliable and widely used energy storage system, where their functioning/behavior at different levels is described by fundamental laws of physics such as, mass transport, electromagnetism, and thermodynamics.

The performance of Li-ion batteries must be nevertheless further improved in terms of energy and power density, by relying on a deeper understanding of their operation principles. In this scope, theoretical simulation at different levels is playing an increasing role in designing, optimizing, and predicting battery performance.

The theoretical simulation of the battery at different levels from the sub-atomic (nano) scale to the macro-scale allows the selection, optimization, and prediction of different properties including the selection and amounts of active material in the electrodes, geometrical effects, or properties of the separator membranes, the performance of each component being described through the different equations that govern its functioning.

In lithium-ion batteries, the battery separator is an important component that affects their behavior, being within the scope of recent theoretical simulation works focusing on separator parameters such as morphology, ion transport, mechanical properties, and dendrites growth.

The perspectives for further theoretical works on battery separators are focused on the effect of the interface with the electrodes, ion concentration gradients, and varying morphologies to prevent dendrites growth, among others.

Considering the recent works for this component, it results evident that more theoretical works are still needed addressing the former issues, supported by the increasing number of available data and ML algorithms.

Theoretical simulation will allow a decrease in resources and time consumption in next-generation battery development, leading to a more sustainable and rapid evolution of energy storage systems. Theoretical simulation will thus play a central role in the selection of materials, improving the safety and performance of the new generation of lithium-ion batteries with a focus on sustainability.

Future battery science and engineering should foster interdisciplinary collaboration allowing to overcome the current issues on battery development and properly address one of the global problems of our time in the scope of energy transition and sustainability.

## Acknowledgements

The authors thank the FCT (Fundação para a Ciência e Tecnologia) for financial support under the framework of Strategic Funding grants

UIDB/04650/2020, UID/FIS/04650/2020, UID/QUI/0686/2020, UID/EEA/04436/2020, UIDB/05549/2020, UIDP/05549/2020, and LASI-LA/P/0104/2020, project PTDC/FIS-MAC/28157/2017, MIT-EXPL/TDI/0033/2021 and project SmartHealth, "NORTE-01-0145-FEDER-000045", supported by Northern Portugal Regional Operational Programme (Norte2020), under the Portugal 2020 Partnership Agreement, through the European Regional Development Fund (ERDF). The authors also thank the FCT for financial support under Investigator FCT Contracts CEECIND/00833/2017 (R.G.) and 2020.04028.CEECIND (C.M.C.) as well POCH and European Union. Financial support from the Basque Government Industry Department under the ELKARTEK program was also acknowledged. This study forms part of the Advanced Materials programme and was supported by MCIN with funding from European Union NextGenerationEU (PRTR-C17.I1) and by Basque Government.

## Conflict of Interest

The authors declare no conflict of interest.

## Keywords

electrochemical models, lithium-ion batteries, modeling, separators, theoretical simulation, thermal models

Received: November 14, 2022
Revised: December 9, 2022
Published online: February 15, 2023

[1] a) R. A. Kerr, R. F. Service, *Science* **2005**, *309*, 101; b) J. P. Holdren, *Science* **2007**, *315*, 737.
[2] J. M. Tarascon, M. Armand, *Nature* **2001**, *414*, 359.
[3] N. Nitta, F. Wu, J. T. Lee, G. Yushin, *Mater. Today* **2015**, *18*, 252.
[4] G. Pistoia, *Lithium-Ion Batteries: Advances and Applications*, Elsevier Science, Amsterdam **2013**.
[5] a) Z. Wang, J. Ni, L. Li, J. Lu, *Cell Rep. Phys. Sci.* **2020**, *1*, 100078; b) A. Y. S. Eng, C. B. Soni, Y. Lum, E. Khoo, Z. Yao, S. K. Vineeth, V. Kumar, J. Lu, C. S. Johnson, C. Wolverton, Z. W. Seh, *Sci. Adv.* **2022**, *8*, eabm2422; c) D. Miranda, C. M. Costa, S. Lanceros-Mendez, *J. Electroanal. Chem.* **2015**, *739*, 97.
[6] P. M. Gomadam, J. W. Weidner, R. A. Dougal, R. E. White, *J. Power Sources* **2002**, *110*, 267.
[7] E. Martínez-Rosas, R. Vasquez-Medrano, A. Flores-Tlacuahuac, *Comput. Chem. Eng.* **2011**, *35*, 1937.
[8] a) L. Cai, R. E. White, *J. Power Sources* **2011**, *196*, 5985; b) P. W. C. Northrop, M. Pathak, D. Rife, S. De, S. Santhanagopalan, V. R. Subramanian, *J. Electrochem. Soc.* **2015**, *162*, A940; c) S. Bae, H. D. Song, I. Nam, G.-P. Kim, J. M. Lee, J. Yi, *Chem. Eng. Sci.* **2014**, *118*, 74; d) R. E. Gerver, J. P. Meyers, *J. Electrochem. Soc.* **2011**, *158*, A835.
[9] A. Bates, S. Mukherjee, N. Schuppert, B. Son, J. G. Kim, S. Park, *Int. J. Energy Res.* **2015**, *39*, 1505.
[10] a) A. A. Franco, M. L. Doublet, W. G. Bessler, *Physical Multiscale Modeling and Numerical Simulation of Electrochemical Devices for Energy Conversion and Storage: From Theory to Engineering to Practice*, Springer, London **2015**; b) V. Ramadesigan, P. W. C. Northrop, S. De, S. Santhanagopalan, R. D. Braatz, V. R. Subramanian, *J. Electrochem. Soc.* **2012**, *159*, R31.
[11] Y. S. Meng, M. E. Arroyo-de Dompablo, *Energy Environ. Sci.* **2009**, *2*, 589.
[12] A. Muralidharan, M. I. Chaudhari, L. R. Pratt, S. B. Rempe, *Sci. Rep.* **2018**, *8*, 10736.
[13] E. W. C. Spotte-Smith, S. M. Blau, X. Xie, H. D. Patel, M. Wen, B. Wood, S. Dwaraknath, K. A. Persson, *Sci. Data* **2021**, *8*, 203.
[14] E. M. Gavilán-Arriazu, M. P. Mercer, D. E. Barraco, H. E. Hoster, E. P. M. Leiva, *Prog. Energy* **2021**, *3*, 042001.
[15] S. Hu, Y. Li, K. M. Rosso, M. L. Sushko, *J. Phys. Chem. C* **2013**, *117*, 28.
[16] K.-S. Yun, S. J. Pai, B. C. Yeo, K.-R. Lee, S.-J. Kim, S. S. Han, *J. Phys. Chem. Lett.* **2017**, *8*, 2812.
[17] a) X. Chen, Q. Zhang, *Acc. Chem. Res.* **2020**, *53*, 1992; b) X. Chen, X. Q. Zhang, H. R. Li, Q. Zhang, *Batteries Supercaps* **2019**, *2*, 128.
[18] O. Borodin, X. Ren, J. Vatamanu, A. von Wald Cresce, J. Knap, K. Xu, *Acc. Chem. Res.* **2017**, *50*, 2886.
[19] a) Z.-H. Fu, X. Chen, C.-Z. Zhao, H. Yuan, R. Zhang, X. Shen, X.-X. Ma, Y. Lu, Q.-B. Liu, L.-Z. Fan, Q. Zhang, *Energy Fuels* **2021**, *35*, 10210; b) A. M. Nolan, Y. Zhu, X. He, Q. Bai, Y. Mo, *Joule* **2018**, *2*, 2016.
[20] C. R. Groom, I. J. Bruno, M. P. Lightfoot, S. C. Ward, *Acta Crystallogr. B* **2016**, *72*, 171.
[21] M. Hellenbrandt, *Crystallogr. Rev.* **2004**, *10*, 17.
[22] J. E. Saal, S. Kirklin, M. Aykol, B. Meredig, C. Wolverton, *JOM* **2013**, *65*, 1501.
[23] A. Jain, S. P. Ong, G. Hautier, W. Chen, W. D. Richards, S. Dacek, S. Cholia, D. Gunter, D. Skinner, G. Ceder, K. A. Persson, *APL Mater.* **2013**, *1*, 011002.
[24] C. Chen, Y. Zuo, W. Ye, X. Li, Z. Deng, S. P. Ong, *Adv. Energy Mater.* **2020**, *10*, 1903242.
[25] W. Sha, Y. Guo, Q. Yuan, S. Tang, X. Zhang, S. Lu, X. Guo, Y.-C. Cao, S. Cheng, *Adv. Intell. Syst.* **2020**, *2*, 1900143.
[26] a) R. Batra, L. Song, R. Ramprasad, *Nat. Rev. Mater.* **2021**, *6*, 655; b) M. Meuwly, *Chem. Rev.* **2021**, *121*, 10218.
[27] G. H. Gu, J. Noh, I. Kim, Y. Jung, *J. Mater. Chem. A* **2019**, *7*, 17096.
[28] A. Chen, X. Zhang, Z. Zhou, *InfoMat* **2020**, *2*, 553.
[29] T. Lombardo, M. Duquesnoy, H. El-Bouysidy, F. Årén, A. Gallo-Bueno, P. B. Jørgensen, A. Bhowmik, A. Demortière, E. Ayerbe, F. Alcaide, M. Reynaud, J. Carrasco, A. Grimaud, C. Zhang, T. Vegge, P. Johansson, A. A. Franco, *Chem. Rev.* **2022**, *122*, 10899.
[30] S. Li, J. Li, H. He, H. Wang, *Energy Procedia* **2019**, *159*, 168.
[31] X. Chen, X. Liu, X. Shen, Q. Zhang, *Angew. Chem., Int. Ed.* **2021**, *60*, 24354.
[32] a) A. Bhowmik, I. E. Castelli, J. M. Garcia-Lastra, P. B. Jørgensen, O. Winther, T. Vegge, *Energy Storage Mater.* **2019**, *21*, 446; b) A. Jain, G. Hautier, S. P. Ong, K. Persson, *J. Mater. Res.* **2016**, *31*, 977; c) D. H. Barrett, A. Haruna, *Curr. Opin. Electrochem.* **2020**, *21*, 160.
[33] S. Russell, P. Norvig, *Artificial Intelligence: A Modern Approach*, Prentice Hall, New Jersey **2002**.
[34] R. P. Joshi, J. Eickholt, L. Li, M. Fornari, V. Barone, J. E. Peralta, *ACS Appl. Mater. Interfaces* **2019**, *11*, 18494.
[35] O. Allam, B. W. Cho, K. C. Kim, S. S. Jang, *RSC Adv.* **2018**, *8*, 39414.
[36] X. Wang, R. Xiao, H. Li, L. Chen, *J. Materiomics* **2017**, *3*, 178.
[37] M. Attarian Shandiz, R. Gauvin, *Comput. Mater. Sci.* **2016**, *117*, 270.
[38] R. A. Eremin, P. N. Zolotarev, O. Y. Ivanshina, I. A. Bobrikov, *J. Phys. Chem. C* **2017**, *121*, 28293.
[39] R. P. Cunha, T. Lombardo, E. N. Primo, A. A. Franco, *Batteries Supercaps* **2020**, *3*, 60.
[40] Y. Takagishi, T. Yamanaka, T. Yamaue, *Batteries* **2019**, *5*, 54.
[41] S. Müller, C. Sauter, R. Shunmugasundaram, N. Wenzler, V. De Andrade, F. De Carlo, E. Konukoglu, V. Wood, *Nat. Commun.* **2021**, *12*, 6205.
[42] H. Xu, M. Zhu, J. Marcicki, X. G. Yang, *J. Power Sources* **2017**, *345*, 137.
[43] J. Huber, C. Tammer, S. Krotil, S. Waidmann, X. Hao, C. Seidel, G. Reinhart, *Proc. CIRP* **2016**, *57*, 585.
[44] K. Sodeyama, Y. Igarashi, T. Nakayama, Y. Tateyama, M. Okada, *Phys. Chem. Chem. Phys.* **2018**, *20*, 22585.

[45] R. Jalem, M. Nakayama, T. Kasuga, *J. Mater. Chem. A* **2014**, *2*, 720.
[46] S. Ibrahim, M. R. Johan, *Int. J. Electrochem. Sci.* **2011**, *6*, 5565.
[47] N. Kireeva, V. S. Pervov, *Phys. Chem. Chem. Phys.* **2017**, *19*, 20904.
[48] B. Liu, J. Yang, H. Yang, C. Ye, Y. Mao, J. Wang, S. Shi, J. Yang, W. Zhang, *J. Mater. Chem. A* **2019**, *7*, 19961.
[49] K. Fujimura, A. Seko, Y. Koyama, A. Kuwabara, I. Kishida, K. Shitara, C. A. J. Fisher, H. Moriwake, I. Tanaka, *Adv. Energy Mater.* **2013**, *3*, 980.
[50] A. Gayon-Lombardo, L. Mosser, N. P. Brandon, S. J. Cooper, *npj Comput. Mater.* **2020**, *6*, 82.
[51] T. Gao, W. Lu, *J. Electrochem. Soc.* **2020**, *167*, 110519.
[52] S. Zhu, N. Zhao, J. Sha, *Energy Storage* **2019**, *1*, e98.
[53] W. Li, J. Zhu, Y. Xia, M. B. Gorji, T. Wierzbicki, *Joule* **2019**, *3*, 2703.
[54] X. Tang, K. Yao, B. Liu, W. Hu, F. Gao, *Energies* **2018**, *11*, 86.
[55] K. A. Severson, P. M. Attia, N. Jin, N. Perkins, B. Jiang, Z. Yang, M. H. Chen, M. Aykol, P. K. Herring, D. Fraggedakis, M. Z. Bazant, S. J. Harris, W. C. Chueh, R. D. Braatz, *Nat. Energy* **2019**, *4*, 383.
[56] D. Gao, M. Huang, *J. Power Electron.* **2017**, *17*, 756.
[57] a) J. Wei, G. Dong, Z. Chen, *IEEE Trans. Ind. Electron.* **2018**, *65*, 5634; b) H. Dong, X. Jin, Y. Lou, C. Wang, *J. Power Sources* **2014**, *271*, 114; c) Y. Cheng, C. Lu, T. Li, L. Tao, *Energy* **2015**, *90*, 1983; d) Y. Zhang, Q. Tang, Y. Zhang, J. Wang, U. Stimming, A. A. Lee, *Nat. Commun.* **2020**, *11*, 1706; e) M. A. Patil, P. Tagade, K. S. Hariharan, S. M. Kolake, T. Song, T. Yeo, S. Doo, *Appl. Energy* **2015**, *159*, 285; f) D. Yang, X. Zhang, R. Pan, Y. Wang, Z. Chen, *J. Power Sources* **2018**, *384*, 387; g) T. Zahid, K. Xu, W. Li, C. Li, H. Li, *Energy* **2018**, *162*, 871.
[58] a) T. F. Fuller, M. Doyle, J. Newman, *J. Electrochem. Soc.* **1994**, *141*, 1; b) M. Doyle, T. F. Fuller, J. Newman, *J. Electrochem. Soc.* **1993**, *140*, 1526; c) M. Doyle, J. Newman, A. S. Gozdz, C. N. Schmutz, J. M. Tarascon, *J. Electrochem. Soc.* **1996**, *143*, 1890.
[59] G. F. Kennell, R. W. Evitts, *Adv. Chem. Eng. Sci.* **2012**, *2*, 12.
[60] a) M. Tang, P. Albertus, J. Newman, *J. Electrochem. Soc.* **2009**, *156*, A390; b) K. Eberman, P. Gomadam, G. Jain, E. Scott, *ECS Trans.* **2010**, *25*, 47.
[61] D. Miranda, C. M. Costa, A. M. Almeida, S. Lanceros-Méndez, *Solid State Ionics* **2015**, *278*, 78.
[62] a) G. Inoue, H. Mashioka, Y. Tsuge, *ECS Meet. Abstr.* **2018**, *MA2018-02*, 206; b) F. Röder, S. Sonntag, D. Schröder, U. Krewer, *Energy Technol.* **2016**, *4*, 1588.
[63] G. Sikha, B. N. Popov, R. E. White, *J. Electrochem. Soc.* **2004**, *151*, A1104.
[64] a) S. J. Cooper, D. S. Eastwood, J. Gelb, G. Damblanc, D. J. L. Brett, R. S. Bradley, P. J. Withers, P. D. Lee, A. J. Marquis, N. P. Brandon, P. R. Shearing, *J. Power Sources* **2014**, *247*, 1033; b) M. Ebner, D.-W. Chung, R. E. García, V. Wood, *Adv. Energy Mater.* **2014**, *4*, 1301278.
[65] K. K. Patel, J. M. Paulsen, J. Desilvestro, *J. Power Sources* **2003**, *122*, 144.
[66] a) M. Park, X. Zhang, M. Chung, G. B. Less, A. M. Sastry, *J. Power Sources* **2010**, *195*, 7904; b) H. Wolf, Z. Pajkic, T. Gerdes, M. Willert-Porada, *J. Power Sources* **2009**, *190*, 157; c) Y. G. Chirkov, V. I. Rostokin, A. M. Skundin, *Russ. J. Electrochem.* **2011**, *47*, 1239; d) S. Yu, Y. Chung, M. S. Song, J. H. Nam, W. I. Cho, *J. Appl. Electrochem.* **2012**, *42*, 443; e) Y. H. Chen, C. W. Wang, X. Zhang, A. M. Sastry, *J. Power Sources* **2010**, *195*, 2851; f) G. Sikha, R. E. White, *J. Electrochem. Soc.* **2008**, *155*, A893.
[67] C. M. Costa, M. M. Silva, S. Lanceros-Méndez, *RSC Adv.* **2013**, *3*, 11404.
[68] U. Sahapatsombut, H. Cheng, K. Scott, *J. Power Sources* **2013**, *243*, 409.
[69] C. Cai, D. Hensley, G. M. Koenig, *J. Energy Storage* **2022**, *54*, 105218.
[70] G. J. Nelson, B. N. Cassenti, A. A. Peracchio, W. K. S. Chiu, *J. Electrochem. Soc.* **2012**, *159*, A598.
[71] J. Association for Chemical Innovation, *Computer Simulation of Polymeric Materials: Applications of the OCTA System*, Springer, Berlin/Heidelberg, Germany **2016**.
[72] D. V. Horváth, R. Tian, C. Gabbett, V. Nicolosi, J. N. Coleman, *J. Electrochem. Soc.* **2022**, *169*, 030503.
[73] D. Miranda, C. M. Costa, A. M. Almeida, S. Lanceros-Méndez, *Appl. Energy* **2016**, *165*, 318.
[74] D. Miranda, C. M. Costa, A. M. Almeida, S. Lanceros-Méndez, *J. Electroanal. Chem.* **2016**, *780*, 1.
[75] R. Zhao, S. Zhang, J. Liu, J. Gu, *J. Power Sources* **2015**, *299*, 557.
[76] D. Miranda, C. M. Costa, A. M. Almeida, S. Lanceros-Méndez, *Energy* **2018**, *149*, 262.
[77] K. Shah, D. Chalise, A. Jain, *J. Power Sources* **2016**, *330*, 167.
[78] S. Golmon, K. Maute, M. L. Dunn, *Comput. Struct.* **2009**, *87*, 1567.
[79] B. Suthar, V. Ramadesigan, S. De, R. D. Braatz, V. R. Subramanian, *Phys. Chem. Chem. Phys.* **2014**, *16*, 277.
[80] P. Singh, N. Khare, P. K. Chaturvedi, *Int. J. Eng. Sci. Technol.* **2018**, *21*, 35.
[81] a) L. Sheng, X. Xie, C. Arbizzani, L. Bargnesi, Y. Bai, G. Liu, H. Dong, T. Wang, J. He, *J. Membr. Sci.* **2022**, *657*, 120644; b) X. Dai, X. Zhang, J. Wen, C. Wang, X. Ma, Y. Yang, G. Huang, H.-M. Ye, S. Xu, *Energy Storage Mater.* **2022**, *51*, 638.
[82] a) P. Arora, Z. Zhang, *Chem. Rev.* **2004**, *104*, 4419; b) C. M. Costa, Y.-H. Lee, J.-H. Kim, S.-Y. Lee, S. Lanceros-Méndez, *Energy Storage Mater.* **2019**, *22*, 346; c) J. Nunes-Pereira, C. M. Costa, S. Lanceros-Méndez, *J. Power Sources* **2015**, *281*, 378; d) C. M. Costa, E. Lizundia, S. Lanceros-Méndez, *Prog. Energy Combust. Sci.* **2020**, *79*, 100846; e) J. Xing, J. Li, W. Fan, T. Zhao, X. Chen, H. Li, Y. Cui, Z. Wei, Y. Zhao, *Composites, Part B* **2022**, *243*, 110105.
[83] K. Xu, *Chem. Rev.* **2004**, *104*, 4303.
[84] a) L. Ding, D. Li, F. Du, D. Zhang, S. Zhang, R. Xu, T. Wu, *J. Power Sources* **2022**, *543*, 231838; b) J. Im, J. Ahn, J. Y. Kim, E. J. Park, S. Yoon, Y.-G. Lee, K. Y. Cho, *Chem. Eng. J.* **2022**, *450*, 138159.
[85] a) X. Huang, *J. Solid State Electrochem.* **2011**, *15*, 649; b) V. Deimede, C. Elmasides, *Energy Technol.* **2015**, *3*, 453; c) Y. Wu, F. Yang, Y. Cao, M. Xiang, J. Kang, T. Wu, Q. Fu, *Polymer* **2021**, *230*, 124081; d) T. Wu, K. Wang, M. Xiang, Q. Fu, *Chin. J. Chem.* **2019**, *37*, 1207.
[86] a) K. Bicy, A. B. Gueye, D. Rouxel, N. Kalarikkal, S. Thomas, *Surf. Interfaces* **2022**, *31*, 101977; b) Y. Li, Q. Li, Z. Tan, *J. Power Sources* **2019**, *443*, 227262.
[87] a) T.-H. Cho, M. Tanaka, H. Ohnishi, Y. Kondo, M. Yoshikazu, T. Nakamura, T. Sakai, *J. Power Sources* **2010**, *195*, 4272; b) J. Hao, G. Lei, Z. Li, L. Wu, Q. Xiao, L. Wang, *J. Membr. Sci.* **2013**, *428*, 11.
[88] a) J.-W. Lee, A. M. Soomro, M. Waqas, M. A. U. Khalid, K. H. Choi, *Int. J. Energy Res.* **2020**, *44*, 7035; b) C.-H. Chao, C.-T. Hsieh, W.-J. Ke, L.-W. Lee, Y.-F. Lin, H.-W. Liu, S. Gu, C.-C. Fu, R.-S. Juang, B. C. Mallick, Y. A. Gandomi, C.-Y. Su, *J. Power Sources* **2021**, *482*, 228896.
[89] a) C. Cheng, H. Liu, C. Ouyang, N. Hu, G. Zha, H. Hou, *Compos. Commun.* **2022**, *33*, 101217; b) A. J. Manly, W. E. Tenhaeff, *J. Mater. Chem. A* **2022**, *10*, 10557.
[90] a) R. R. Jacquemond, C. T.-C. Wan, Y.-M. Chiang, Z. Borneman, F. R. Brushett, K. Nijmeijer, A. Forner-Cuenca, *Cell Rep. Phys. Sci.* **2022**, *3*, 100943; b) X. Yao, X. Song, F. Zhang, J. Ma, H. Jiang, L. Wang, Y. Liu, E. Huixiang Ang, H. Xiang, *ChemElectroChem* **2022**, *9*, 202200390.
[91] X. Xie, L. Sheng, R. Xu, X. Gao, L. Yang, Y. Gao, Y. Bai, G. Liu, H. Dong, X. Fan, T. Wang, X. Huang, J. He, *J. Electroanal. Chem.* **2022**, *920*, 116570.
[92] a) Z. Wang, J. Chen, S. Sun, Z. Huang, X. Zhang, X. Li, H. Dong, *Energy Storage Mater.* **2022**, *50*, 161; b) J. Y. Kim, D. Y. Lim, *Energies* **2010**, *3*, 866.

[93] Y. Min, L. Guo, G. Wei, D. Xian, B. Zhang, L. Wang, *Chem. Eng. J.* **2022**, *443*, 136480.
[94] W. Chen, X. Wang, J. Liang, Y. Chen, W. Ma, S. Zhang, *Membranes* **2022**, *12*, 124.
[95] S. H. Kang, H. Y. Jeong, T. H. Kim, J. Y. Lee, S. K. Hong, Y. T. Hong, J. Choi, S. So, S. J. Yoon, D. M. Yu, *Polymers* **2022**, *14*, 1649.
[96] J. Gou, W. Liu, A. Tang, L. Wu, *J. Membr. Sci.* **2022**, *659*, 120807.
[97] M. Li, K. Wang, J. Liu, F. Shen, C. Xu, X. Han, *J. Colloid Interface Sci.* **2022**, *622*, 1029.
[98] X. Li, K. Liu, Y. Yan, J. Yu, N. Dong, B. Liu, G. Tian, S. Qi, D. Wu, *J. Colloid Interface Sci.* **2022**, *625*, 936.
[99] Y. D. Lee, J. Yuenyongsuwan, P. Nanthananon, Y. K. Kwon, *Polymer* **2022**, *255*, 125110.
[100] J. Liu, D. Cao, H. Yao, D. Liu, X. Zhang, Q. Zhang, L. Chen, S. Wu, Y. Sun, D. He, J. Liu, *ACS Appl. Energy Mater.* **2022**, *5*, 8639.
[101] X. Gao, L. Sheng, M. Li, X. Xie, L. Yang, Y. Gong, M. Cao, Y. Bai, H. Dong, G. Liu, T. Wang, X. Huang, J. He, *ACS Appl. Polym. Mater.* **2022**, *4*, 5125.
[102] M. Qiao, G. Zhang, J. Deng, J. Guo, J. Zhang, *J. Mater. Sci.* **2022**, *57*, 11796.
[103] W. Tang, Q. Liu, N. Luo, F. Chen, Q. Fu, *Compos. Sci. Technol.* **2022**, *225*, 109479.
[104] H. Jeong, J. Hwang, J. Kim, W.-J. Song, K. J. Lee, *Mater. Chem. Phys.* **2022**, *288*, 126354.
[105] A. J. Manly, W. E. Tenhaeff, *Electrochim. Acta* **2022**, *425*, 140705.
[106] W. Wang, A. C. Y. Yuen, Y. Yuan, C. Liao, A. Li, I. I. Kabir, Y. Kan, Y. Hu, G. H. Yeoh, *Chem. Eng. J.* **2023**, *451*, 138496.
[107] S. Nag, A. Pramanik, S. Roy, S. Mahanty, *J. Solid State Chem.* **2022**, *312*, 123214.
[108] Y. Pan, L.-Y. He, X.-Y. Qiu, X. Li, *J. Electron. Mater.* **2022**, *51*, 4307.
[109] L. Yu, J. Gu, C. Pan, J. Zhang, Z. Wei, Y. Zhao, *Composites, Part A* **2022**, *162*, 107132.
[110] W. Zhai, H. Yu, H. Chen, L. Li, D. Li, Y. Zhang, T. He, *Sep. Purif. Technol.* **2022**, *293*, 121091.
[111] Y. Yang, N. Li, T. Lv, Z. Chen, Y. Liu, K. Dong, S. Cao, T. Chen, *Nanoscale Adv.* **2022**, *4*, 1718.
[112] a) E. Lizundia, C. M. Costa, R. Alves, S. Lanceros-Méndez, *Carbohydr. Polym. Technol. Appl.* **2020**, *1*, 100001; b) H. Zhang, S. Wang, A. Wang, Y. Li, F. Yu, Y. Chen, *Appl. Surf. Sci.* **2022**, *593*, 153411; c) Y. Xie, H. Zhu, R. Zeng, B. Na, S. Zou, C. Chen, *J. Power Sources* **2022**, *538*, 231562; d) X. Zheng, J. Wu, X. Wang, Z. Yang, *Chem. Eng. J.* **2022**, *446*, 137194.
[113] a) R. F. P. Pereira, R. Brito-Pereira, R. Gonçalves, M. P. Silva, C. M. Costa, M. M. Silva, V. de Zea Bermudez, S. Lanceros-Méndez, *ACS Appl. Mater. Interfaces* **2018**, *10*, 5385; b) A. Reizabal, R. Gonçalves, A. Fidalgo-Marijuan, C. M. Costa, L. Pérez, J.-L. Vilas, S. Lanceros-Mendez, *J. Membr. Sci.* **2020**, *598*, 117678.
[114] A. Reizabal, A. Fidalgo-Marijuan, R. Gonçalves, A. Gutiérrez-Pardo, F. Aguesse, L. Pérez-Álvarez, J. L. Vilas-Vilela, C. M. Costa, S. Lanceros-Mendez, *J. Colloid Interface Sci.* **2022**, *611*, 366.
[115] a) W. Xiao, L. Zhao, Y. Gong, J. Liu, C. Yan, *J. Membr. Sci.* **2015**, *487*, 221; b) L. Ding, N. Yan, S. Zhang, R. Xu, T. Wu, F. Yang, Y. Cao, M. Xiang, *Electrochim. Acta* **2022**, *403*, 139568; c) N. Kassenova, S. Kalybekkyzy, M. V. Kahraman, A. Mentbayeva, Z. Bakenov, *J. Power Sources* **2022**, *520*, 230896.
[116] A. Liu, Z. Jiang, S. Li, J. Du, Y. Tao, J. Lu, Y. Cheng, H. Wang, *Int. J. Biol. Macromol.* **2022**, *213*, 690.
[117] J. P. Serra, A. Fidalgo-Marijuan, J. Teixeira, L. Hilliou, R. Gonçalves, K. Urtiaga, A. Gutiérrez-Pardo, F. Aguesse, S. Lanceros-Mendez, C. M. Costa, *Adv. Sustainable Syst.* **2022**, *6*, 2200279.
[118] Y. Chen, J. Li, Y. Ju, R. Cheng, Y. Zhai, J. Sheng, H. Liu, L. Li, *Appl. Surf. Sci.* **2022**, *592*, 153222.
[119] a) Y. Feng, M. Wang, L. Gao, Z. He, K. Chen, Z. Li, H. He, Y. Lin, *J. Materiomics* **2022**, *8*, 1184; b) S. Ahankari, D. Lasrado, R. Subramaniam, *Mater. Adv.* **2022**, *3*, 1472.
[120] M. Kim, J. K. Kim, J. H. Park, *Adv. Funct. Mater.* **2015**, *25*, 3399.
[121] Y. Kang, C. Deng, Z. Wang, Y. Chen, X. Liu, Z. Liang, T. Li, Q. Hu, Y. Zhao, *Nanoscale Res. Lett.* **2020**, *15*, 107.
[122] a) E. Shekarian, M. R. Jafari Nasr, T. Mohammadi, O. Bakhtiari, M. Javanbakht, *J. Appl. Polym. Sci.* **2019**, *136*, 47841; b) W. Jiang, Y. Han, Y. Ding, *Nanotechnology* **2022**, *33*, 425601.
[123] a) J. Li, L. Chen, F. Wang, Z. Qin, Y. Zhang, N. Zhang, X. Liu, G. Chen, *Chem. Eng. J.* **2023**, *451*, 138536; b) X. Wu, C. Zhou, C. Dong, C. Shen, B. Shuai, C. Li, Y. Li, Q. An, X. Xu, L. Mai, *Nano Res.* **2022**, *15*, 8048; c) A. Valverde, R. Gonçalves, M. M. Silva, S. Wuttke, A. Fidalgo-Marijuan, C. M. Costa, J. L. Vilas-Vilela, J. M. Laza, M. I. Arriortua, S. Lanceros-Méndez, R. Fernández de Luis, *ACS Appl. Energy Mater.* **2020**, *3*, 11907; d) R. Freund, O. Zaremba, G. Arnauts, R. Ameloot, G. Skorupskii, M. Dincă, A. Bavykina, J. Gascon, A. Ejsmont, J. Goscianska, M. Kalmutzki, U. Lächelt, E. Ploetz, C. S. Diercks, S. Wuttke, *Angew. Chem., Int. Ed.* **2021**, *60*, 23975.
[124] a) S. Aadheeshwaran, K. Sankaranarayanan, V. Ganesh, *Ionics* **2021**, *27*, 607; b) Y. Luo, H. Bai, B. Li, X. Song, J. Zhao, Y. Xiao, S. Lei, B. Cheng, *J. Alloys Compd.* **2021**, *879*, 160368.
[125] D. Cao, J. Deng, L. Jiang, X. Li, G. Zhang, *J. Energy Storage* **2022**, *55*, 105496.
[126] Y. Min, X. Liu, L. Guo, A. Wu, D. Xian, B. Zhang, L. Wang, *ACS Appl. Energy Mater.* **2022**, *5*, 9131.
[127] J. C. Barbosa, R. Gonçalves, A. Valverde, P. M. Martins, V. I. Petrenko, M. Márton, A. Fidalgo-Marijuan, R. Fernández de Luis, C. M. Costa, S. Lanceros-Méndez, *Chem. Eng. J.* **2022**, *443*, 136329.
[128] A. A. Franco, A. Rucci, D. Brandell, C. Frayret, M. Gaberscek, P. Jankowski, P. Johansson, *Chem. Rev.* **2019**, *119*, 4569.
[129] K. Shah, V. Vishwakarma, A. Jain, *J. Electrochem. Energy Convers. Storage* **2016**, *13*, 030801.
[130] W. Xie, Y. Dang, L. Wu, W. Liu, A. Tang, Y. Luo, *Polym. Test.* **2020**, *90*, 106773.
[131] Y. Kawagoe, D. Surblys, G. Kikugawa, T. Ohara, *AIP Adv.* **2019**, *9*, 025302.
[132] S. Yan, X. Xiao, X. Huang, X. Li, Y. Qi, *Polymer* **2014**, *55*, 6282.
[133] Y. Saito, W. Morimura, R. Kuratani, S. Nishikawa, *J. Phys. Chem. C* **2016**, *120*, 3619.
[134] R. Zahn, M. F. Lagadec, M. Hess, V. Wood, *ACS Appl. Mater. Interfaces* **2016**, *8*, 32637.
[135] A. Ehrl, J. Landesfeind, W. A. Wall, H. A. Gasteiger, *J. Electrochem. Soc.* **2017**, *164*, A2716.
[136] K. Yoo, A. Deshpande, S. Banerjee, P. Dutta, *Electrochim. Acta* **2015**, *176*, 301.
[137] V. Zadin, D. Danilov, D. Brandell, P. H. L. Notten, A. Aabloo, *Electrochim. Acta* **2012**, *65*, 165.
[138] M. F. Lagadec, R. Zahn, S. Müller, V. Wood, *Energy Environ. Sci.* **2018**, *11*, 3194.
[139] C. Sauter, R. Zahn, V. Wood, *J. Electrochem. Soc.* **2020**, *167*, 100546.
[140] a) M. Gilaki, I. Avdeev, *J. Power Sources* **2016**, *328*, 443; b) S. Kalnaus, A. Kumar, Y. Wang, J. Li, S. Simunovic, J. A. Turner, P. Gorney, *J. Power Sources* **2018**, *378*, 139.
[141] R. Gonçalves, T. Marques-Almeida, D. Miranda, M. M. Silva, V. F. Cardoso, C. M. Costa, S. Lanceros-Méndez, *Energy Storage Mater.* **2019**, *21*, 124.
[142] R. Gonçalves, D. Miranda, T. Marques-Almeida, M. M. Silva, V. F. Cardoso, A. M. Almeida, C. M. Costa, S. Lanceros-Méndez, *J. Colloid Interface Sci.* **2021**, *596*, 158.
[143] P. Priimägi, H. Kasemägi, A. Aabloo, D. Brandell, V. Zadin, *Electrochim. Acta* **2017**, *244*, 129.
[144] Y.-k. Ahn, J. Park, D. Shin, S. Cho, S. Y. Park, H. Kim, Y. Piao, J. Yoo, Y. S. Kim, *J. Mater. Chem. A* **2015**, *3*, 10715.
[145] D. Shi, X. Xiao, X. Huang, H. Kia, *J. Power Sources* **2011**, *196*, 8129.

[146] M. Zhuo, D. Grazioli, A. Simone, *Electrochim. Acta* **2021**, *393*, 139045.
[147] a) X. Xiao, W. Wu, X. Huang, *J. Power Sources* **2010**, *195*, 7649; b) W. Wu, X. Xiao, X. Huang, S. Yan, *Comput. Mater. Sci.* **2014**, *83*, 127.
[148] X. Zhang, E. Sahraei, K. Wang, *J. Power Sources* **2016**, *327*, 693.
[149] D. Grazioli, V. Zadin, D. Brandell, A. Simone, *Electrochim. Acta* **2018**, *296*, 1142.
[150] M. F. Lagadec, R. Zahn, V. Wood, *J. Electrochem. Soc.* **2018**, *165*, A1829.
[151] A. Jana, D. R. Ely, R. E. García, *J. Power Sources* **2015**, *275*, 912.
[152] H. Xu, C. Bae, *J. Power Sources* **2019**, *430*, 67.
[153] D. Sauerteig, N. Hanselmann, A. Arzberger, H. Reinshagen, S. Ivanov, A. Bund, *J. Power Sources* **2018**, *378*, 235.
[154] Y. Li, G. Zhang, B. Chen, W. Zhao, L. Sha, D. Wang, J. Yu, S. Shi, *Chin. Chem. Lett.* **2022**, *33*, 3287.
[155] A. Cannon, E. M. Ryan, *ACS Appl. Energy Mater.* **2021**, *4*, 7848.
[156] J. Liang, Q. Chen, X. Liao, P. Yao, B. Zhu, G. Lv, X. Wang, X. Chen, J. Zhu, *Angew. Chem., Int. Ed.* **2020**, *59*, 6561.

**Daniel Miranda** graduated in Physics and Chemistry in 2005 and obtained his Master's Degree in Physics in 2008. In 2017, he received a Ph.D. in Physics from the Science School of the University of Minho. Currently, he is an Adjunct Professor invited at School of Technology, Polytechnic Institute of Cávado and Ave (IPCA), Portugal, and integrated member/researcher of 2Ai Laboratory at IPCA. His work focuses on the development of theoretical models of lithium-ion batteries through computational simulation (Finite Elements Method) and computational simulation and modeling applied in energy, energy systems, and storage energy applications.

**Renato Gonçalves**, Ph.D., has a background in Chemistry and Chemistry Analysis Characterization Techniques and obtained his Ph.D. degree in Materials Engineering (2017) at the University of Minho, Portugal. Since 2019, he is working at Chemistry Centre of the University of Minho, Portugal as a researcher being involved in various national and international research projects and scientific international collaborations (Cambridge, Jodhpur, Bilbao). His current research interest involves the development of materials, synthesis, and printing techniques for advanced applications and new energy storage materials, including Lithium-ion batteries. He has published more than 80 papers and book chapters as author and co-author.

**Stefan Wuttke** created the research group "WuttkeGroup for Science", initially hosted at the Institute of Physical Chemistry at the University of Munich (LMU, Germany). Currently, he is an Ikerbasque Professor at the Basque Center for Materials, Applications, and Nanostructures (BCMaterials, Spain). His principal focus is the design, synthesis, and functionalization of MOFs and their nanometric counterparts to target diverse applications. At the same time, he aims to establish a basic understanding of the chemical and physical elementary processes involved in the synthesis, functionalization, and application of these hybrid materials.

**Carlos M. Costa** graduated in Physics in 2005 and obtained his Master's Degree in Materials Engineering in 2007. In 2014, he received a Ph.D. in Physics from the Science School of the University of Minho. Currently, He is an Assistant researcher at the Center of Physics of the same university. His work focuses on the development of sustainable materials for sensors and actuators as well as on the development of electroactive polymer-based porous membranes, anode and cathode material for energy storage applications: lithium-ion batteries, printed batteries.

**Senentxu Lanceros-Mendez** is Ikerbasque Professor at BCMaterials, Basque Center for Materials, Applications and Nanostructures, Leioa, Spain, where he is the Scientific Director. He is an Associate Professor at the Physics Department of the University of Minho, Portugal (on leave), which also belongs to the Center of Physics. He graduated in Physics at the University of the Basque Country, Leioa, Spain and obtained his Ph.D. degree at the Institute of Physics of the Julius-Maximilians-Universität Würzburg, Germany. His work is focused on the development of smart and multifunctional materials for sensors and actuators, energy, environmental, and biomedical applications.